AD-A035 908 DAVID W TAYLOR NAVAL SHIP RESEARCH AND DEVELOPMENT CE--ETC F/G 13/10
EXPERIMENTAL INVESTIGATION OF HYDRODYNAMIC COEFFICIENTS OF A SM--ETC(U)
JAN 77 C M LEE, L O MURRAY

UNCLASSIFIED SPD-747-01 NL

1 OF 1
AD-A
035 908

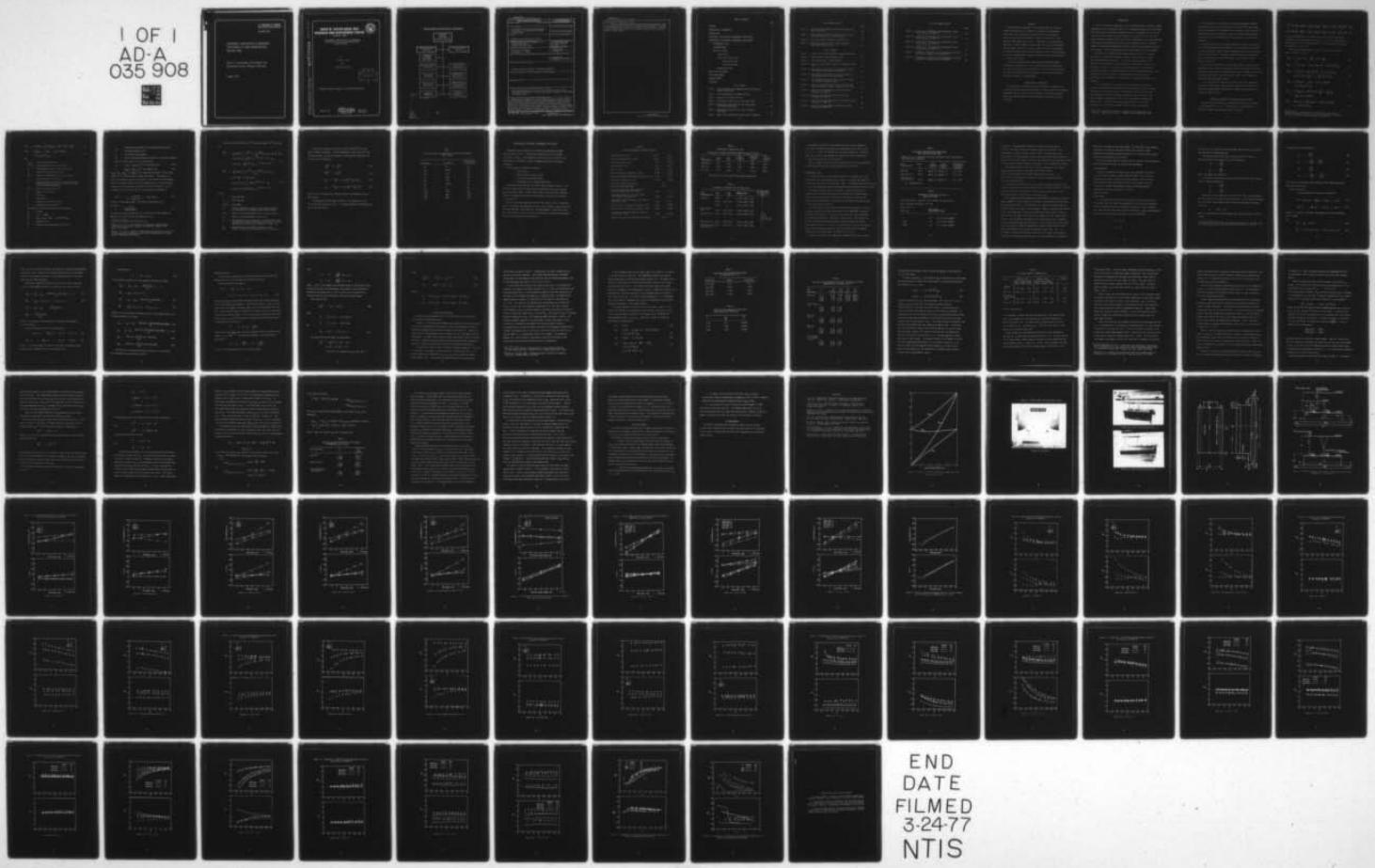

END
DATE
FILMED
3-24-77
NTIS

U.S. DEPARTMENT OF COMMERCE
National Technical Information Service

AD-A035 908

EXPERIMENTAL INVESTIGATION OF HYDRODYNAMIC COEFFICIENTS OF A SMALL-WATERPLANE-AREA TWIN-HULL MODEL

DAVID W. TAYLOR NAVAL SHIP RESEARCH AND DEVELOPMENT CENTER, BETHESDA, MARYLAND

JANUARY 1977

EXPERIMENTAL INVESTIGATION OF HYDRODYNAMIC COEFFICIENTS OF A SMALL WATERPLANE AREA, TWIN-HULL MODEL
ADA035908
Report No. SPD 747-01

DAVID W. TAYLOR NAVAL SHIP RESEARCH AND DEVELOPMENT CENTER

Bethesda, Md. 20084

EXPERIMENTAL INVESTIGATION OF HYDRODYNAMIC COEFFICIENTS OF A SMALL-WATERPLANE-AREA, TWIN-HULL MODEL

by

Choung M. Lee

and

Lawrence O. Murray

DDC
RECEIVED
FEB 23 1977
A

APPROVED FOR PUBLIC RELEASE: DISTRIBUTION UNLIMITED

January 1977

REPRODUCED BY
NATIONAL TECHNICAL
INFORMATION SERVICE
U. S. DEPARTMENT OF COMMERCE
SPRINGFIELD, VA. 22161

Report No.
SPD 747-01

MAJOR DTNSRDC ORGANIZATIONAL COMPONENTS

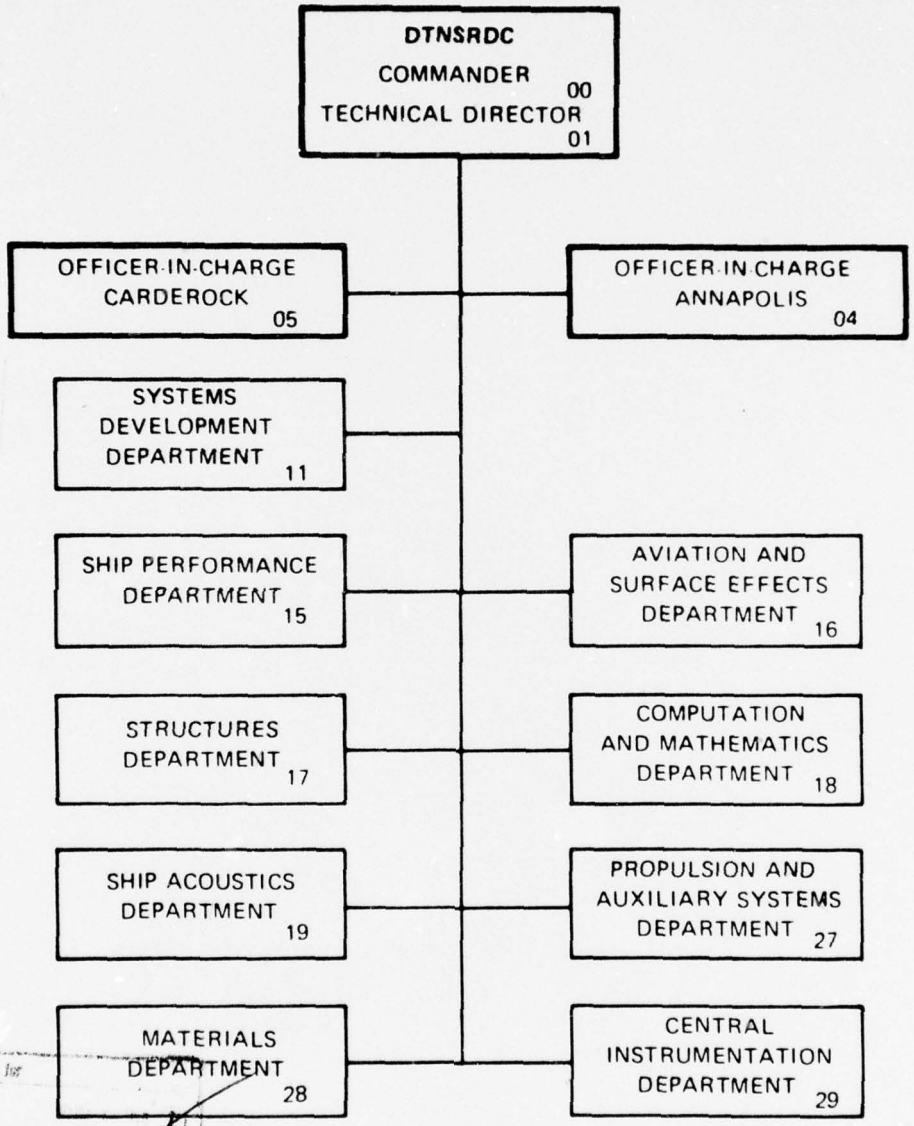

ACCESSION for
NTIS
DDC
A

UNCLASSIFIED

SECURITY CLASSIFICATION OF THIS PAGE (When Data Entered)

REPORT DOCUMENTATION PAGE		READ INSTRUCTIONS BEFORE COMPLETING FORM
1. REPORT NUMBER	2. GOVT ACCESSION NO.	3. RECIPIENT'S CATALOG NUMBER
4. TITLE (and Subtitle) Experimental Investigation of Hydrodynamic Coefficients of a Small-Waterplane-Area, Twin-Hull Model		5. TYPE OF REPORT & PERIOD COVERED 6. PERFORMING ORG. REPORT NUMBER
7. AUTHOR(s) Choung M. Lee and Lawrence O. Murray		8. CONTRACT OR GRANT NUMBER(s)
9. PERFORMING ORGANIZATION NAME AND ADDRESS David W. Taylor Naval Ship Research and Development Center Bethesda, Maryland 20084		10. PROGRAM ELEMENT, PROJECT, TASK AREA & WORK UNIT NUMBERS Task Area SF43421202 Task 18247 Work Unit 1-1507-200
11. CONTROLLING OFFICE NAME AND ADDRESS Naval Material Command Washington, D.C. 20360		12. REPORT DATE January 1977 13. NUMBER OF PAGES 87
14. MONITORING AGENCY NAME & ADDRESS(if different from Controlling Office)		15. SECURITY CLASS. (of this report) Unclassified 15a. DECLASSIFICATION/DOWNGRADING SCHEDULE

16. DISTRIBUTION STATEMENT (of this Report)

APPROVED FOR PUBLIC RELEASE: DISTRIBUTION UNLIMITED

17. DISTRIBUTION STATEMENT (of the abstract entered in Block 20, if different from Report)

18. SUPPLEMENTARY NOTES

19. KEY WORDS (Continue on reverse side if necessary and identify by block number)

Small-Waterplane-Area Twin-Hull Ships; Ship Motions in Waves; Ship Hydrodynamic Coefficients; Fin-Body Interactions, Comparison of Experimental and Computed Values

20. ABSTRACT (Continue on reverse side if necessary and identify by block number)

Experiments were conducted on a small waterplane area, twin-hull (SWATH) model designated as SWATH 6A to determine the hydrodynamic coefficients associated with the following fin-body combinations: bare hull, bare hull with forward fin, bare hull with aft fin, and bare hull with forward and aft fins. Three types of experiments were conducted at several speeds: calm-water towing for various fixed drafts and trim angles, forced oscillation in both the pitch and heave modes, and towing in regular head waves. The objective of the investigation was to verify the computational methods utilized for predicting

DD FORM 1 JAN 73 1473 EDITION OF 1 NOV 65 IS OBSOLETE
S/N 0102-014-6601

UNCLASSIFIED

SECURITY CLASSIFICATION OF THIS PAGE (When Data Entered)

the motions of a SWATH ship in waves.

In general agreement between measured and computed hydrodynamic coefficients confirmed the validity of the computational method used. The study also provided valuable insight for improving both the methods of computing the hydrodynamic coefficients and the method of measuring the forces and moments of SWATH models.

TABLE OF CONTENTS

	Page
ABSTRACT	1
ADMINISTRATIVE INFORMATION	1
INTRODUCTION	2
THEORETICAL PREDICTION OF HYDRODYNAMIC COEFFICIENTS	3
EXPERIMENTALLY DETERMINED HYDRODYNAMIC COEFFICIENTS	10
EXPERIMENTAL SETUP	13
INSTRUMENTATION	16
ANALYSIS OF DATA	16
Static Tests	16
Forced Oscillation Tests	18
Heave Oscillations	18
Pitch Oscillations	19
Regular-Wave Tests	21
RESULTS AND DISCUSSION	23
CONCLUDING REMARKS	39
ACKNOWLEDGMENTS	40
REFERENCES	41

LIST OF TABLES

Table 1 - Dividing Factors for Nondimensionalizing the Hydrodynamic Coefficients 9

Table 2 - Principal Dimensions of SWATH 6A Model 11

Table 3 - Dimensions of Stabilizing Fins 12

Table 4 - Experimental Conditions for the Static Tests 12

Table 5 - Experimental Conditions for Forced Heave and Pitch Oscillation Tests 14

Table 6 - Experimental Conditions for Tests in Regular Head Waves 14

Table 7 - Heave and Pitch Restoring Coefficients of SWATH 6A 26

LIST OF TABLE (Cont'd)

Page

Table 8 - Equivalent Heave Added Mass Coefficient Found From Static Trim Tests 26

Table 9 - Heave and Pitch Restoring Coefficients for Various Fin-Body Combinations at Different Speeds 27

Table 10 - Lift-Curve Slope per Radian of Various Fins 29

Table 11 - Values of C_{55} Used in Equation (36) to Obtain Experimental Values of A_{55} 36

LIST OF FIGURES

Figure 1 - Values of Lift Ratios Based On Slender Body Theory . . . 42

Figure 2 - SWATH 6A Model and Experimental Setup 43

Figure 3 - Top and Side Views of SWATH 6A Model 45

Figure 4 - Details of Experimental Setup for Forced Oscillation Tests 46

Figure 5 - Pitch Moment and Vertical Force versus Trim Angle for Various Configurations of SWATH 6A 47

Figure 6 - Pitch Moment and Vertical Force versus Draft for SWATH 6A Bare Hull at Various Speeds 52

Figure 7 - Pitch Moment and Vertical Force versus Trim Angle for SWATH 6A at Several Speeds 53

Figure 8 - Effect of Deflection Angle of Aft Fin A on Pitch Moment and Vertical Force of SWATH 6A at F_n=0.384 . . . 56

Figure 9 - Heave and Pitch Added Mass Coefficients versus Frequency for SWATH 6A 57

Figure 10 - Heave and Pitch Damping Coefficients versus Frequency for SWATH 6A 60

Figure 11 - Heave-Pitch Coupling Added Mass Coefficients versus Frequency for SWATH 6A 63

Figure 12 - Hull-Pitch Coupling Damping Coefficients versus Frequency for SWATH 6A 66

LIST OF FIGURES (Cont'd)

Page

Figure 13 - Comparison of Theoretical and Experimental Values of A_{33} and A_{55} for SWATH 6A 69

Figure 14 - Comparison of Theoretical and Experimental Values of B_{33} and B_{55} for SWATH 6A 72

Figure 15 - Comparison of Theoretical and Experimental Values of A_{35} and A_{53} for SWATH 6A 75

Figure 16 - Comparison of Theoretical and Experimental Values of B_{35} and B_{53} for SWATH 6A 78

Figure 17 - Comparison of Theoretical and Experimental Amplitudes and Phases of Wave-Exciting Heave Force 81

Figure 18 - Comparison of Theoretical and Experimental Amplitudes and Phases of Wave-Exciting Pitch Moment. 82

ABSTRACT

Experiments were conducted on a small waterplane area, twin-hull (SWATH) model designated as SWATH 6A to determine the hydrodynamic coefficients associated with the following fin-body combinations: bare hull, bare hull with forward fin, bare hull with aft fin, and bare hull with forward and aft fins. Three types of experiments were conducted at several speeds: calm-water towing for various fixed drafts and trim angles, forced oscillation in both the pitch and heave modes, and towing in regular head waves. The objective of the investigation was to verify the computational methods utilized for predicting the motions of a SWATH ship in waves.

In general agreement between measured and computed hydrodynamic coefficients confirmed the validity of the computational method used. The study also provided valuable insight for improving both the methods of computing the hydrodynamic coefficients and the method of measuring the forces and moments of SWATH models.

ADMINISTRATIVE INFORMATION

This project was sponsored by the Naval Sea Systems Command as part of the High Performance Vehicle Hydrodynamic Program of the Ship Performance Department, David W. Taylor Naval Ship Research and Development Center. Funding was provided under Task Area SF43421202, Task 18247, Work Unit 1-1507-200.

INTRODUCTION

One of the potential advantages of a small-waterplane-area, twin-hull (SWATH) configuration over conventional ships is its seakeeping performance at high speeds. Two factors that provide good seakeeping qualities in moderate seas are (1) the relatively larger natural periods of SWATH ships in the heave, pitch and roll modes compared to monohull ships of equivalent displacement, and (2) the relatively small wave-exciting vertical force due to the submerged main hulls of SWATHs. However, the aforesaid advantage was found to be true only when stabilizing fins are attached. The fins provide necessary vertical-plane stability and damping.

Development of the SWATH concept necessitated the capability to predict the behavior of SWATH configurations in waves. Such an analytical method has been developed and described.[1] Its validity largely depends on the accuracy of the evaluation of the hydrodynamic coefficients involved in the equations of motion. The validity of computed hydrodynamic coefficients is normally assessed by comparing predicted values with experimental data. The present work is aimed at verifying the methods used in evaluating the coefficients and, furthermore, in finding ways to improve the evaluation, if necessary.

It is a formidable task to determine the hydrodynamic coefficients of a SWATH configuration with the degree of accuracy needed to provide reliable predictions of its motion in waves. Consideration must be given not only the hydrodynamic interactions between the two hulls but also to the interactions between the body and the fins and to the interaction between the separate fins. The free surface and unsteady effects of the lifting characteristics of the fins are other difficult problems encountered.

---

[1] Lee, C.M., "Theoretical Prediction of Motion of Small-Waterplane-Area, Twin-Hull (SWATH) Ships in Waves," DTNSRDC Report 76-0046 (Dec. 1976)

It was impossible to include all of the above hydrodynamic effects in the theoretical calculation of the coefficients by using the present state of development in fluid mechanics. Accordingly, various assumptions and approximations were necessary in order to evaluate the hydrodynamic coefficients, and so the reliability of the theoretical values needs to be checked.

The reliability of the calculation methods was checked by experiments with a SWATH model designated as SWATH 6A. The experiments were designed to enable examination of the specific hydrodynamic effects of significance under various conditions. The present report examines only those hydrodynamic coefficients involved in the linear, coupled heave and pitch equations of motion.

The first section describes the analytical methods of evaluating the hydrodynamic coefficients involved in the heave-pitch equations of motion. The second section describes the experimental setup, procedures, and analysis of the measured values. The third section compares and discusses the theoretical and experimental results.

It was found from this study that in general the linear heave-pitch equations of motion used in the calculation methods are satisfactory for predicting the hydrodynamic coefficients of SWATH configurations with horizontal stabilizing fins.

THEORETICAL PREDICTION OF HYDRODYNAMIC COEFFICIENTS

The added mass coefficients A_{ij}, damping coefficients B_{ij}, and wave-exciting forces $F_i^{(e)}$ for $i, j = 3$ and 5 appear in the equations of motion for coupled heave and pitch motion as follows:

$$(M + A_{33})\ddot{\xi}_3 + B_{33}\dot{\xi}_3 + C_{33}\xi_3 + A_{35}\ddot{\xi}_5 + B_{35}\dot{\xi}_5 + C_{35}\xi_5 = F_3^{(e)} e^{-j\omega t} \quad (1)$$

$$(I_5 + A_{55})\ddot{\xi}_5 + B_{55}\dot{\xi}_5 + C_{55}\xi_5 + A_{53}\ddot{\xi}_3 + B_{53}\dot{\xi}_3 + C_{53}\xi_3 = F_5^{(e)} e^{-j\omega t} \quad (2)$$

M and I_5 are respectively the displaced mass of the ship and pitch moment of inertia, not including the mass of the fins, ξ_3 and ξ_5 are heave and pitch displacement from the initial mean position, C_{ij} are the hydrostatic restoring coefficients, and $j = \sqrt{-1}$.

The subscripted coefficients A, B and $F^{(e)}$ are obtained by strip theory as (Table 4 in Lee[1]*).

$$A_{33} = \int_L a_{33}(x)\,dx + \sum_{i=1}^{N} \left(m_i^{(f)} + a_{33i}^{(f)} \right) \quad (3)$$

$$B_{33} = \int_L b_{33}(x)\,dx + \rho a_0 U \int B_m(x)\,dx + \rho U \sum_i A_i^{(f)} C_{L\alpha i} \quad (4)$$

$$A_{35} = -\int x\, a_{33}\,dx - \frac{U}{\omega^2}\int b_{33}\,dx - \frac{\rho}{\omega^2} a_0 U^2 \int B_m\,dx - \sum \ell_i \left(m_i^{(f)} + a_{33i}^{(f)} \right) - \rho \frac{U^2}{\omega^2} \sum A_i^{(f)} C_{L\alpha i} \quad (5)$$

$$B_{35} = -\int x\, b_{33}\,dx + U A_{33} - \rho a_0 U \int x B_m\,dx - \rho U \sum \ell_i A_i^{(f)} C_{L\alpha i} \quad (6)$$

$$A_{55} = \int x^2 a_{33}\,dx + \sum \ell_i^2 \left(m_i^{(f)} + a_{33i}^{(f)} \right) + \frac{U^2}{\omega^2} A_{33} + \frac{\rho}{\omega^2} a_0 U^2 \int x B_m\,dx \quad (7)$$

$$B_{55} = \int x^2 b_{33}\,dx + \frac{U^2}{\omega^2}\int b_{33}\,dx + \rho a_0 U \int x^2 B_m\,dx + \rho U \sum \ell_i^2 A_i^{(f)} C_{L\alpha i} \quad (8)$$

*For the sake of a more straightforward experimental data analysis, a transfer of some terms from C_{ij} to A_{ij} is made by multiplying the terms by $(-1/\omega^2)$, and the cross-flow drag terms are neglected.

$$A_{53} = -\int x a_{33}\, dx + \frac{U}{\omega^2}\int b_{33}\, dx - \sum \ell_i \left(m_i^{(f)} + a_{33_i}^{(f)}\right) \tag{9}$$

$$B_{53} = -\int x b_{33}\, dx - U A_{33} - \rho a_0 U \int x B_m\, dx - \rho U \sum \ell_i A_i^{(f)} C_{L\alpha_i} \tag{10}$$

where

$a_{33}(x)$ = sectional heave added mass

$a^{(f)}_{33i}$ = heave added mass of a pair of the ith fin

A_i = projected plane area of a pair of the ith fin

a_o = viscous lift coefficient (= 0.07)

$B_m(x)$ = diameter of submerged hull at a cross section

$C_{L\alpha i}$ = lift-curve slope of the ith fin

ℓ_i = longitudinal distance from LCG to the quarter-chord point of the ith fin; positive if the fin is forward of LCG and negative otherwise

$m_i^{(f)}$ = mass of a pair of the ith fin

N = number of fins per hull

U = ship speed

ρ = water density

ω = frequency of oscillation of ship

$\int_L$ = integration over ship length

The hydrostatic restoring coefficients are obtained by:

$C_{33} = \rho g A_w$

$C_{35} = C_{53} = \rho g M_w$

$C_{55} = \rho g \forall (I_w/\forall - \overline{BG}) - \rho U^2 \sum \ell_i A_i^{(f)} C_{L\alpha_i}$

A_w = waterplane area

M_w = waterplane area moment about the pitch axis

I_w = waterplane area moment of inertia about the pitch axis

$\forall$ = displaced volume of ship

g = gravitational acceleration

$\overline{BG}$ = vertical distance between the centers of gravity and buoyancy

The lift curve slope of a fin is obtained by

$$C_{L\alpha} = (K_{w(B)} + K_{B(w)}) C_{L\alpha}^{(o)} \quad \text{for stationary fins} \tag{11a}$$

$$C_{L\alpha} = (k_{w(B)} + k_{B(w)}) C_{L\alpha}^{(o)} \quad \text{for movable fins} \tag{11b}$$

$K_{w(B)}$, $K_{B(w)}$, $k_{w(B)}$, and $k_{B(w)}$ can be obtained from Figure 1* which shows values of lift ratios based on slender body theory.[2] The abscissa of Figure 1 represents the ratio r/r_o where r is the radius of the submerged hull cross section at which the fin is attached and r_o is the transverse distance from the centerline of the hull to the tip of the fin. $C_{L\alpha}^{(o)}$ represents the lift-curve slope of fin alone which is obtained by

$$C_{L\alpha}^{(o)} = \frac{1.8\,\pi\,A_e}{1.8 + \sqrt{A_e^2 + 4}} \quad \text{per radian} \tag{12}$$

for fins without sweep angle. The effective aspect ratio A_e is defined by

$$A_e = \frac{r_o - r^2/r_o^2}{\text{average chord}} \tag{13}$$

The expression given by Equation (12) is identical to that obtained by Whicker and Fehlner[3] except the definition of A_e.

---

*Figures are grouped at the end of the text.

[2]Pitts, W.C. et al., "Lift and Center of Pressures of Wing-Body-Tail Combinations at Subsonic, Transonic, and Supersonic Speeds," NACA Report 1307 (1959)

[3]Whicker, L.F. and L.F. Fehlner, "Free-Stream Characteristics of Family of Low-Aspect-Ratio, All-Movable Control Surfaces for Application to Ship Design," DTMB Report 933 (1958).

The wave-exciting heave force $F_3^{(e)}$ and pitch moment $F_5^{(e)}$ are given by

$$F_3^{(e)} = -\frac{j}{\omega_o}\rho g A \int_L e^{-jK_o x}\,dx \int_{C(x)} e^{K_o z} N_3 (j\omega_o + K_o \phi_3')\,dl$$
$$- j\rho\omega_o A a_o U \int_L B_m(x)\, e^{-K_o(d_1(x) + jx)}\,dx$$
$$- j\rho\omega_o A U \sum_{i=1}^{N} A_i^{(f)} C_{L\alpha i}\, e^{-K_o(d_{1i} + j\ell_i)} \qquad (14)$$

$$F_5^{(e)} = -\frac{j}{\omega_o}\rho g A \int_L e^{-jK_o x}\,dx \int_{C(x)} e^{K_o z} N_3 \left[-j\omega_o x + K_o\left(\frac{U}{j\omega} - x\right)\phi_3'\right] dl$$
$$+ j\rho\omega_o A a_o U \int_L x B_m\, e^{-K_o(d_1 + jx)}\,dx \qquad (15)$$
$$+ j\rho\omega_o A U \sum_i \ell_i A_i^{(f)} C_{L\alpha i}\, e^{-K_o(d_{1i} + j\ell_i)}$$

where

A = wave amplitude

ω_o = wave frequency

$K_o = \frac{\omega_o^2}{g}$ = wave number

N_3 = vertical component of the unit normal vector pointing into the body on the submerged cross-section contour

$d_1(x)$ = depth of the maximum breadth point of a cross section

d_{1i} = depth of the mean thickness of the ith fin

ϕ'_3 = two-dimensional velocity potential representing the fluid disturbances caused by forced heave oscillation of a cross section (see the definition in Appendix 1 of Ref. [1]

$\int_{C(x)}$ = integration over the immersed contour of a cross section of both hulls at the mean position of the ship

As given by Equations (14) and (15), $F_3^{(e)}$ and $F_5^{(e)}$ are in the form of complex amplitudes. The real amplitudes, $F_{30}^{(e)}$ and $F_{50}^{(e)}$ and the phase angles α_3 and α_5 with respect to the wave crest above the LCG of the ship are obtained by

$$F_{30}^{(e)} = |F_3^{(e)}| \tag{16}$$

$$F_{50}^{(e)} = |F_5^{(e)}| \tag{17}$$

$$\alpha_3 = \tan^{-1}(-\mathrm{Im}\, F_3^{(e)} / \mathrm{Re}\, F_3^{(e)}) \tag{18}$$

$$\alpha_5 = \tan^{-1}(-\mathrm{Im}\, F_5^{(e)} / \mathrm{Re}\, F_5^{(e)}) \tag{19}$$

where Re and Im, respectively, indicate the real and imaginary parts of what follows.

The hydrodynamic coefficients obtained in the foregoing are non-dimensionalized as shown in Table 1. An overbar denotes the nondimensional form of the coefficient.

TABLE 1

Dividing Factors for Nondimensionalizng the Hydrodynamic Coefficients

Coefficient	Divided by	Nondimensional Coefficient
A_{33}	$\rho\forall$	$\bar{A}_{33}$
B_{33}	$\rho\forall\sqrt{g/L}$	$\bar{B}_{33}$
A_{35}	$\rho\forall L$	$\bar{A}_{35}$
B_{35}	$\rho\forall\sqrt{gL}$	$\bar{B}_{35}$
A_{55}	$\rho\forall L^2$	$\bar{A}_{55}$
B_{55}	$\rho\forall L\sqrt{gL}$	$\bar{B}_{55}$
A_{53}	$\rho\forall L$	$\bar{A}_{53}$
B_{53}	$\rho\forall\sqrt{gL}$	$\bar{B}_{53}$
$F_{30}^{(e)}$	$\frac{\rho\forall gA}{L}$	$\bar{F}_{30}^{(e)}$
$F_{50}^{(e)}$	$\rho\forall gA$	$\bar{F}_{50}^{(e)}$

EXPERIMENTALLY DETERMINED HYDRODYNAMIC COEFFICIENTS

Experiments were conducted with a SWATH model designated as SWATH 6A; see Figures 2 and 3. The principal characteristics of the model are given in Table 2. The dimensions of the stablizing fins used in the experiments are indicated in Table 3 together with their longitudinal locations.

The experiments included the following:

1. Static tests.
2. Forced pitch oscillation tests.
3. Forced heave oscillation tests.
4. Towed model tests in regular head waves.

Experimental conditions for the static tests are shown in Table 4. The bare hull configuration provided restoring coefficients C_{33}, C_{35}, C_{53} and C_{55} at different speeds. The hull with forward fin was tested to determine the lift and moment contributed by the forward fin and to verify Equations (11a) and (11b).

The hull was tested separately with aft fin A and aft fin B to determine the lift and moment contributed by aft fins to two different aspect ratios and to verify Equations (11a,b) and (12). The configuration consisting of the hull with forward fin and aft fin A was investigated to determine the downwash effects of the forward fin on the aft fin.

TABLE 2

Principal Dimensions of SWATH 6A Model

Actual Weight, kg (lb)	254.47		(561)
Displaced Water Weight, kg (lb)	249.93		(551)
Main Hull Length, m (ft)	3.25		(10.67)
Strut Length, m (ft)	2.33		(7.66)
Draft, m (ft)	0.361		(1.19)
Beam of One Hull at Waterline, m (ft)	0.098		(0.32)
Separation between Centerlinesof Two Hull, m (ft)	1.016		(3.33)
Maximum Hull Diameter, m (ft)	0.203		(0.667)
Main Hull Prismatic Coefficient		0.85	
Waterplane Area Coefficient		0.85	
Longitudinal Distance from Nose of Main Hull to Forward Strut End, m (ft)	0.376		(1.23)
Longitudinal Distance from Tail of Main Hull to Rear Strut End, m (ft)	0.542		(1.78)
Longitudinal Center of Buoyancy from Nose of Main Hull, m (ft)	1.576		(5.17)
Vertical Center of Buoyancy from Keel, m (ft)	0.151		(0.496)
Vertical Center of Gravity from Keel, m (ft)	0.562		(1.516)
Longitudinal Center of Flotation from Nose of Main Hull, m (ft)	1.566		(5.14)
Radius of Gyration for Pitch/Main Hull Length		0.221	

TABLE 3

DIMENSIONS OF STABILIZING FINS

(Rectangular Planform with Modified NACA 16 Series Section)

Fin Designation	Chord cm	Span cm	Max Thickness cm	Projected Fin Area cm^2	Fin Location* cm
Forward Fin	11.51	13.82	1.72	159.1	76.2
Aft Fin A	19.91	23.83	2.98	474.5	276.6
Aft Fin B	11.51	23.83	1.72	274.3	276.6

*Distance from the hull nose to the quarter-chord point

TABLE 4

EXPERIMENTAL CONDITIONS FOR THE STATIC TESTS

Hull Configuration	Draft cm	Trim deg	FROUDE NUMBER F_n	Fin Deflection at 0-Deg Trim deg
Bare Hull	29.80	0	0, 0.192, 0.384, 0.538	0
	36.12	0, $\pm$1.5, $\pm$3.0	0.192, 0.384, 0.538	0
	43.35	0	0.192, 0.384, 0.538	0
With Forward Fin	36.12	0, $\pm$1.5, $\pm$3.0	0.192, 0.384, 0.538	0
With Aft Fin A	36.12	0, $\pm$1.5, $\pm$3.0	0.192, 0.384, 0.538	0, $\pm$5, $\pm$10, $\pm$15 at F_n = 0.384
With Aft Fin B	36.12	0, $\pm$1.5, $\pm$3.0	0.192, 0.384, 0.538	0
With Forward Fin and Aft Fin A	36.12	0, $\pm$1.5, $\pm$3.0	0.192, 0.384, 0.538	0

Experimental conditions for the forced oscillation tests (Table 5) were chosen to determine the added mass and damping coefficients A_{ij} and B_{ij} for i,j = 3 and 5 for the bare hull with and without fins in order to check the validity of the theoretical evaluations of these coefficients as expressed by Equations (3) through (10).

Tests in regular wave (Table 6) were conducted to verify the evaluations of $F_3^{(e)}$ and $F_5^{(e)}$ which are given by Equations (14) and (15).

EXPERIMENTAL SETUP

For both the static and the regular wave tests, the model was rigidly attached to the carriage by two vertical struts. The model was towed with fixed drafts and trims during the static tests. The desired drafts and trims were set by using adjustable-length struts between the pivots and the carriage mounts.

For tests in regular waves, an ultrasonic probe was placed 6.78 m ahead of the LCG and used to measure the amplitude of the incoming waves. The aft strut was connected to the vertical oscillator at rest and the forward strut was attached to a fixed point of the towing carriage as shown in the lower portion of Figure 3.

For the forced oscillation tests, the model was connected by a vertical strut to a harmonic oscillator designated as the DTNSRDC MARK II Vertical Oscillator; see Figure 4. The strut was connected to a scotch yoke which was electrically driven by a horizontal rotating shaft. The eccentricity of the scotch yoke could be continuously varied to obtain the desired amplitude of oscillation up to 10 cm, and the voltage input to the electric motor could be continuously varied to set the scotch yoke at the desired frequency of oscillation within the range of 0 to 1.2 Hz.

Two block or modular force gages were attached to each strut as shown

TABLE 5

EXPERIMENTAL CONDITIONS FOR FORCED HEAVE AND PITCH OSCILLATION TESTS

(Speeds of F_n = 0, 0.384 and 0.538 were employed for each configuration and experimental condition)

Hull Configuration	Draft cm	Heave Amplitude cm	Pitch Amplitude deg	Frequency of Oscillation (rad/sec)
Bare Hull	36.12	Approx 3.8	Approx 1.5	2.0 - 4.0*
With Aft Fin A	36.12	Approx 3.8	Approx 1.5	2.0 - 4.0*
With Forward Fin and Aft Fin A	36.12	Approx 3.8	Approx 1.5	2.0 - 4.0*

*In increments of 0.2

TABLE 6

EXPERIMENTAL CONDITIONS FOR TESTS IN REGULAR HEAD WAVES

Hull configuration: bare hull with Forward fin and Aft Fin A.

Wave length/Wave amplitude: 120 ~ 300

Draft: 36.12 cm

Speed (F_n)	$\frac{\text{Wave Length}}{\text{Ship Length (3.25m)}}$
0	0.8 ~ 5.0 (11 wave lengths)
0.384	2.5 ~ 7.5 (11 wave lengths)
0.538	2.5 ~ 7.7 (12 wave lengths)

in Figure 4. The measurement capacity of each block gage was 500 lb (226.8 N). One gage (X gage) was oriented to measure longitudinal force and the other (Z gage) to measure vertical force. A single pitch pivot was attached to the forward gage assembly which was placed directly above the center of gravity and a double pitch pivot was attached to the stern gage assembly. The double pivot allowed alignment of the model in the longitudinal direction.

Displacement during the heave oscillation was measured by an ultrasonic probe placed on the deck of the model that emitted acoustic signals to a horizontal rigid plane fixed beneath the carriage. The pitch angular displacement was measured by an angle potentiometer during the pitch oscillation tests.

In the heave-oscillation tests at zero speed, the model was placed transversely to the tank to avoid wave reflections from the tank side walls. Although the same orientation was desirable for the pitch-oscillation test, it was not done because of the difficulty of apparatus setup.

To be compatible with the theoretical prediction which is based on slender-body assumption, it was desirable to eliminate the pitch moment contribution by the longitudinal forces. For SWATH models, the upper deck provides the most practical location to install the force gages. However, unusually high location of the force gages which is about twice the height of the center of gravity from the keel can impose large loads on the Z gages since the Z gages have to restrain the pitch moment contributed by the longitudinal forces in addition to that contributed by the vertical forces. Such an imposition of extra loads due to the drag on Z gages can degrade the accuracy of the analysis of pitch moment contributed by the vertical hydrodynamic forces alone. Thus, in an attempt to reduce the undesirable extra loads on Z gages, the x-componet of forces was minimized by adjusting the rpm of the propellers to counteract

the drag of the model at each towing speed. This was done at each speed by determining the propeller rpm which minimized the resultant X-gage readings while the model was towed with zero trim. The rpm values so determined were used during the towing tests.

Each run was made under the condition that no residual fluid disturbances from the preceding runs were included in the measurements.

INSTRUMENTATION

The main instrumentation system used in the experiments consisted of an on-carriage minicomputer system (Inter Data Model 70), digital and analog tape recorders, TV Monitors and tape recorder, and strip charts. The minicomputer performed harmonic analysis of the motion and force records, and computed the amplitudes, phases, and the hydrodynamic coefficients involved in Equations (1) and (2).

ANALYSIS OF DATA

Static Tests

If the readings from the vertical force gage at the rear strut and at the forward strut are respectively denoted by F_1 and F_2 and the separation distance between the two struts connected to these force gages is denoted by ℓ, then the total heave force F_3 and pitch moment F_5 about the longitudinal center of gravity exerted on the model are easily obtained by

$$F_3 = F_1 + F_2$$

$$F_5 = F_1 \ell$$

The sense of F_3 is taken to be positive upward and that for F_5 as positive when the bow of the model goes down.

The restoring coefficients C_{55} and C_{35} for given trim angles θ that are positive for bow-down trim can be obtained by

$$C_{35} = -\frac{\Delta F_3}{\Delta \theta}$$

$$C_{55} = -\frac{\Delta F_5}{\Delta \theta}$$

where Δ designates the difference.

The restoring coefficients C_{33} and C_{53} are obtained for given sinkages h which are negative downward by

$$C_{33} = -\frac{\Delta F_3}{\Delta h}$$

$$C_{53} = -\frac{\Delta F_5}{\Delta h}$$

Because the X force (drag) was not zero for all runs, the coefficients had to be modified to account for the nonzero drag. If the positive direction of the X force is taken toward the bow, the drag-contributed pitch moment is given by

$$D_5 = -\ell_D(X_1 + X_2)^*$$

where ℓ_D is the vertical distance between the X gages and center of the net X force.

---

*This expression tacitly implies that the drag and thrust are colinear since in reality, there could be the case that $D_5 \neq 0$ even if $X_1 + X_2 = 0$.

The coefficients are now given as

$$C_{35} = - \frac{\Delta F_3}{\Delta \theta} \tag{20}$$

$$C_{55} = - \left(\frac{\Delta F_5}{\Delta \theta} - \frac{\Delta D_5}{\Delta \theta} \right) \tag{21}$$

$$C_{33} = - \frac{\Delta F_3}{\Delta h} \tag{22}$$

$$C_{53} = - \left(\frac{\Delta F_5}{\Delta h} - \frac{\Delta D_5}{\Delta h} \right) \tag{23}$$

These restoring coefficients were obtained at each model towing speed.

Forced Oscillation Tests

Heave Oscillations

The heave equations of motion are expressed by

$$(M' + A_{33}) \ddot{z} + B_{33} \dot{z} + C_{33} z = F_3 (t) \tag{24}$$

$$A_{53} \ddot{z} + B_{53} \dot{z} + C_{53} z = F_5 (t) \tag{25}$$

where M' is the mass of the model and apparatus affecting the readings of the Z gages.

Let

$$z = z_0 \sin \omega t \tag{26}$$

$$F_3 = F_{10} \sin (\omega t + \alpha_1) + F_{20} \sin (\omega t + \alpha_2) \tag{27}$$

Here ω is the oscillation frequency, the subscript 0 indicates the amplitude, subscripts 1 and 2, respectively, designate forces at the aft and forward vertical force gage positions and α is the phase angle which is positive when the force leads the motion.

Substituting Equations (26) and (27) into (24) and (25), replacing F_5 by ℓF_1, and decomposing the cos ωt terms and sin ωt terms, we have

$$A_{33} = \frac{1}{\omega^2}\left(C_{33} - \frac{F_{10}\cos\alpha_1 + F_{20}\cos\alpha_2}{z_0}\right) - M' \qquad (28)$$

$$B_{33} = \frac{1}{\omega z_0}\left(F_{10}\sin\alpha_1 + F_{20}\sin\alpha_2\right) \qquad (29)$$

$$A_{53} = \frac{1}{\omega^2}\left(C_{53} - \frac{\ell F_{10}\cos\alpha_1}{z_0}\right)$$

$$B_{53} = \frac{\ell F_{10}\sin\alpha_1}{\omega z_0}$$

where M' is the mass of the moving parts of the model and apparatus.

Pitch Oscillation

The pitch equations of motion are expressed by

$$(\quad' + A_{55})\ddot{\theta} + B_{55}\dot{\theta} + C_{55}\theta = \ell F_1(t) \qquad (30)$$

$$A_{35}\ddot{\theta} + B_{35}\dot{\theta} + C_{35}\theta = F_3(t) \qquad (31)$$

where I' is the mass moment of inertia of the model and apparatus about the pitch axis through the pivot at the forward strut.

Substitution of

$$\theta = \theta_o \sin \omega t \tag{32}$$

and F_3 given by Equation (27) into Equations (30) and (31) yields

$$A_{55} = \frac{1}{\omega^2} \left(C_{55} - \frac{\ell F_{10} \cos \alpha_1}{\theta_o} \right) - I'$$

$$B_{55} = \frac{1}{\omega \theta_o} \ell F_{10} \sin \alpha_1$$

$$A_{35} = \frac{1}{\omega^2} \left(C_{35} - \frac{F_{10} \cos \alpha_1 + F_{20} \cos \alpha_2}{\theta_o} \right) \tag{33}$$

$$B_{35} = \frac{1}{\omega \theta_o} \left(F_{10} \sin \alpha_1 + F_{20} \sin \alpha_2 \right) \tag{34}$$

Removal of the pitch moment contributed by the X force changes some of the foregoing equations as follows:

$$A_{53} = \frac{1}{\omega^2} \left(C_{53} - \frac{\ell F_{10} \cos \alpha_1 - \ell_D (X_{10} \cos \beta_1 + X_{20} \cos \beta_2)}{z_o} \right) \tag{35}$$

$$A_{55} = \frac{1}{\omega^2} \left(C_{55} - \frac{\ell F_{10} \cos \alpha_1 - \ell_D (X_{10} \cos \beta_1 + X_{20} \cos \beta_2)}{\theta_o} \right) - I' \tag{36}$$

$$B_{53} = \frac{\ell F_{10} \sin \alpha_1 - \ell_D (X_{10} \sin \beta_1 + X_{20} \sin \beta_2)}{\omega z_o} \tag{37}$$

$$B_{55} = \frac{\ell F_{10} \sin \alpha_1 - \ell_D (X_{10} \sin \beta_1 + X_{20} \sin \beta_2}{\omega \theta_o} \tag{38}$$

The added mass and damping coefficients obtained in the foregoing are nondimensionalized according to Table 1.

Regular-Wave Tests

The amplitudes and phases of the wave-exciting heave force and pitch moment about the LCG of the model were obtained as follows.

The heave force was obtained by

$$F_3^{(e)} = F_{30}^{(e)} \sin(\omega t + \alpha_H)$$

$$= F_{10} \sin(\omega t + \alpha_1) + F_{20} \sin(\omega t + \alpha_2) \qquad (39)$$

where F_{10} and F_{20} are respectively the amplitudes of the forces obtained at the aft and forward gage locations. Positive phase angles α_1 and α_2 are the phase leads with respect to the wave nodal point of positive slope above the LCG. Since the wave probe was located 6.78 m ahead of the LCG, an adjustment of phase shift should be made. If we let the distance between the wave probe and the LCG be x_0, then the elevation of progressive plane sinusoidal waves in deep water can be given by

$$\eta = A \sin(\omega t + \frac{\omega_0^2}{g} x_0)$$

where A is the amplitude, and ω_0 the wave frequency which is related to wave length λ by $\omega_0 = (\frac{2\pi g}{\lambda})^{1/2}$. The encounter frequency ω can be obtained for head waves by

$$\omega = \omega_0 + \frac{\omega_0^2}{g} U = \omega_0 + \frac{4\pi^2}{g T_0^2} U$$

where U is the towing speed and T_0 is the wave period.

Thus,

$$\alpha_1 = \alpha_1' - \frac{4\pi^2}{g T_0^2} (x_0 + \ell_1)$$

$$\alpha_2 = \alpha_2' - \frac{4\pi^2}{g T_0^2} (x_0 - \ell_2)$$

where α'_1 and α'_2 are respectively the phase angles of the vertical forces obtained at the aft and forward gages, with respect to the wave motion recorded at the probe, and ℓ_1 (= 72.1 cm) and ℓ_2 (=15.25 cm) are the distances from the LCG to the center of the vertical force gages.

From Equation (39),

$$F_{30}^{(e)} = (F_c^2 + F_s^2)^{\frac{1}{2}} \tag{40}$$

where

$$F_c = F_{10} \cos\alpha_1 + F_{20} \cos\alpha_2$$

$$F_s = F_{10} \sin\alpha_1 + F_{20} \sin\alpha_2$$

and

$$\alpha_H = \tan^{-1} (F_s / F_c) \tag{41}$$

The wave-exciting pitch moment was obtained by

$$F_5^{(e)} = F_{50}^{(e)} \sin(\omega t + \alpha_p)$$

$$= \ell F_{10} \sin(\omega t + \alpha_1)$$

$$- \ell_D [X_{10} \sin(\omega t + \beta_1) + X_{20} \sin(\omega t + \beta_2)]$$

Thus,

$$F_{50}^{(e)} = (F_c'^2 + F_s'^2)^{\frac{1}{2}} \tag{42}$$

$$\alpha_p = \tan^{-1} (F_s' / F_c') \tag{43}$$

where

$$F_c' = \ell F_{10} \cos\alpha_1 - \ell_D (X_{10} \cos\beta_1 + X_{20} \cos\beta_2)$$

$$F_s' = \ell F_{10} \sin\alpha_1 - \ell_D (X_{10} \sin\beta_1 + X_{20} \sin\beta_2)$$

RESULTS AND DISCUSSION

The results are presented first for the static tests, and then for the oscillation and regular-wave tests.

Figures 5a - 5e show the pitch moment and vertical force versus trim angle for various configurations of the model at three forward speeds and Figure 6 indicates the moment and force versus sinkage for the bare hull. Values are given in units of Newton-meters (N-m) and Newton (N) for pitch moment and lift respectively. Straight lines are drawn through experimental points to indicate the slopes. Negative values for measured forces and moment were converted to positive in order to show positive values for the restoring coefficients.

Each portion of Figure 5 shows a different fin-body combination. The slope of the curves in the upper and lower portions of Figures 5a and 6 for $F_n = 0$ should respectively correspond to C_{55}, C_{35}, C_{53}, and C_{33} which are defined below Equation (10). The computed and measured values of these restoring

coefficients are shown in Table 7. Theoretically, for small sinkage and trim C_{35} and C_{53} should be identical. The slight difference found is attributed to inaccuracy in experimental values resulting from the minimum measurement limit of the force gages used (about $\pm$ 0.227 Kg or $\pm$ 0.5 lb).

As can be seen from Figure 5a, the slope of the curve of pitch moment decreased as the speed of the model increased. At F_n = 0.538, the slope becomes zero which means that there is no pitch-restoring capability and thus instability of the body can exist between the speeds F_n = 0.384 and 0.538. The theoretically computed speed of inception of instability[4] in the vertical plane modes was F_n = 0.423. The values of C_{55} obtained from the experiment for the bare hull at F_n = 0.193, 0.348, and 0.538 were respectively 9.3, 3.96, and 0. N-m/deg. The difference in C_{55} at different speeds for the bare hull should be indicative of the so-called Munk moment which is ab out U^2A_{33}. The values of $A_{33}/(\rho V)$ obtained from the differences in C_{55} at the foregoing speeds are shown in Table 8. For a deeply submerged submarine, the values shown in Table 8 correspond to the so-called M'_w (see Gertler and Hagen[5]) which are also shown in Table 8. Experimental data on submarine models show that for the diameter-to-length ratio (0.0625) corresponding only to the body of revolution without the strut of the present model, M'_w is approximately 0.004 for all speeds. The difference between this result and that of the present case may be attributed to the free-surface effect and the difference in the hull geometries.

---

[4]Lee, C.M., and M. Martin, "Determination of Size of Stabilizing Fins for Small Waterplane Area, Twin-Hull Ships," DTNSRDC Report 4495 (1974)

[5]Gertler, M. and G.R. Hagen, "Standard Equations of Motion for Submarine Simulation," DTNSRDC Report 2510 (1967)

The pitch moments shown in the present report are assumed to be contributed by the vertical forces only. The experimental analysis was made by subtracting D_5 which is defined just before Equation (20). The moment arm ℓ_D was taken as the vertical distance between the main body axis to the gage location which was 72.15 cm. This choice of vertical moment arm assumes that the x-component of the hydrodynamic force acts through the main-body axis; unfortunately, there does not seem to be any adequate method to determine the correct value of ℓ_D. For similar future experiments, it is recommended that a better means of determining ℓ_D should be established to avoid similar ambiguity encountered in the present analysis.

The slopes obtained from Figures 5 and 6 are shown in Table 9. The coefficients defined in the frequency domain as shown in Equations (3) and (9) may be approximately converted to the steady case by exchanging the speed-dependent terms in A_{ij} to C_{ij}. When this is done, the restoring coefficients are expressed as

$$C_{33}' = \rho g A_w \tag{44}$$

$$C_{35}' = \rho g M_w + U \int b_{33}\, dx + \rho a_0 U^2 \int B_m\, dx + \rho U^2 \sum A_i^{(f)} C_{L\alpha i} \tag{45}$$

$$C_{53}' = \rho g M_w - U \int b_{33}\, dx \tag{46}$$

$$C_{55}' = \rho g \forall \left(I_w / \forall - \overline{BG} \right) - U^2 A_{33} - \rho a_0 U^2 \int x B_m\, dx - \rho U^2 \sum A_i^{(f)} \ell_i C_{L\alpha i} \tag{47}$$

TABLE 7

HEAVE AND PITCH RESTORING COEFFICIENTS
OF SWATH 6A at $F_n = 0$

Coefficient	Theory	Experiment
$C_{33}L/(\rho g \nabla)$	5.55	5.33
$C_{35}/(\rho g \nabla)$	-0.016	-0.023
$C_{53}/(\rho g \nabla)$	-0.016	-0.027
$C_{55}/(\rho g \nabla L)$	0.093	0.094

TABLE 8

EQUIVALENT HEAVE ADDED MASS COEFFICIENT
FOUND FROM STATIC TRIM TESTS

F_n	$\frac{A_{33}}{\rho \nabla}$	M_w'
0.192	0.74	0.00504
0.384	0.446	0.00325
0.538	0.326	0.00285

TABLE 9

HEAVE AND PITCH RESTORING COEFFICIENTS FOR VARIOUS FIN-BODY COMBINATIONS AT DIFFERENT SPEEDS

Hull Conditions	F_n	C'_{55} N-m/deg	C'_{35} N/deg	C'_{53} N-m/m	C'_{33} N/m
Bare Hull	0	13.12	-0.978	-65.16	3948.9
	0.192	9.30	0	-48.93	3927.9
	0.384	3.95	2.94	-73.39	3742.3
	0.538	0	12.23	85.62	3765.0
With Forward Fin	0				
	0.192	8.64	0.48		
	0.384	2.60	8.91		
	0.538	-2.60	18.41		
With Aft Fin A	0				
	0.192	13.54	4.74		
	0.384	16.52	20.59		
	0.538	33.18	41.42		
With Aft Fin B	0				
	0.192	12.89	5.22		
	0.384	16.30	14.56		
	0.538	28.21	37.19		
With Forward Fin and Aft Fin A	0				
	0.192	12.55	4.81		
	0.384	14.35	21.08		
	0.538	27.07	51.21		

The measured values shown in Table 9 should correspond to the definitions of C'_{ij} given above.

In order to obtain $C_{L\alpha i}$, the values of C_{35} of the bare hull at each speed were subtracted from those of the finned bodies at the corresponding speed, and similarly for C_{55}. Thus,

$$\Delta C_{35} = \rho U^2 \sum A_i^{(f)} C_{L\alpha i} \tag{48}$$

$$\Delta C_{55} = -\rho U^2 \sum \ell_i A_i^{(f)} C_{L\alpha i} \tag{49}$$

from which two values of $C_{L\alpha i}$ can be obtained. The values of lift-curve slope are shown in Table 10. The theoretical values obtained from Equation (11a) are shown in the last column. As can be seen, the values as obtained from Equations (48) and (49) differed considerably. As explained earlier, the theoretical values of $C_{L\alpha i}$ were obtained under various simplified assumptions and therefore, they may not necessarily be be more reliable than the experimental values. The values obtained from Equation (48) exhibited more scatter than those obtained by Equation (49). Intuitively, the values obtained by Equation (48) would be expected to be more reliable than the others; however, the scatter of the data does not support that. The values obtained by Equation (49) at F_n = 0.384 were generally smaller than those at other speeds. The downwash effects of the forward fin on Aft Fin A can be measured approximately. In fact, the two values of $C_{L\alpha}$ for Aft Fin A imply that the downwash effects reduced $C_{L\alpha}$ for the aft fin. Except for the forward fin, the theoretically estimated values seemed to be lower than the experimental values.

TABLE 10

LIFT-CURVE SLOPE* OF VARIOUS FINS

Fin	From Eq. (48)			From Eq. (49)			Theory
	Speed (Froude number)			Speed (Froude number)			
	0.192	0.384	0.538	0.192	0.384	0.538	
Forward Fin	1.46	4.58	2.42	2.24	1.19	1.16	4.38
Aft Fin A	3.86	5.10	3.52	3.74	2.77	3.74	3.20
Aft Fin A (with Forward Fin)	3.50	2.50	4.32	3.45	2.59	3.34	3.20
Aft Fin B	10.50	6.91	6.33	5.52	4.73	5.52	4.75

*Given in "per radian"

An increase in aspect ratio would be expected to yield larger values of $C_{L\alpha}$; this seemed to be the case when the values were compared for Aft Fin A and Aft Fin B. The aspect ratio was about twice as high for Fin B than for Fin A. The value of $C_{L\alpha}$ = 10.50 for Fin B at F_n = 0.192 appears to be unrealistically high.

Figure 6 shows the pitch moment and the vertical force generated on the bare hull at other than the design draft (36.12 cm). The upper portion of the figure shows a sudden change in the sense of pitch moment when the speed increases from F_n = 0.384 to F_n = 0.538. Such a change in the sense of the pitch moment with changes in speed changes is due mainly to the

free-surface effect. An earlier model experiment by Korvin-Kroukovsky, et al[6] and an application of slender-body theory by McCreight[7] have confirmed that the depth of submergence and the speed can significantly change both the magnitude and sense of the pitch moment on a body. The lower portion of Figure 6 shows an almost constant slope for all four speeds. The upper portion provides C_{53} and the lower portion C_{33}; these values are shown in Tables 7 and 9.

Figure 7 shows the pitch moment and the vertical force induced by angles of attack of the body for all the fin-body combinations at the various speeds. The trends of the curves in Figure 7 are as expected. That is, the most effective restoring pitch moment is contributed by the aft fins whereas the most restoring vertical force is contributed by both fins. These trends become more distinct as speed increases. It can be observed from Figure 7c that the forward fin contributes a destabilizing pitch moment when the model speed increases.

Figure 8 indicates the pitch moment and vertical force generated when Aft Fin A is deflected from its zero-angle of attack position, i.e., the fin chord line parallel to the main hull axis. A positive fin angle is defined in the conventional leading-edge-upward position. The body was held at zero trim and sinkage and was towed at a constant speed of $F_n = 0.384$. The lift and the pitch moment contributed by the fin are linear up to 20 degrees for positive

---

[6] Korvin-Kroukovsky, B.V. et al, "Theoretical and Experimental Investigation of the Interaction of a Free Surface and a Body of Revolution Moving under It," Experimental Towing Tank, Stevens Inst. Tech. Report 390 (1950).

[7] McCreight, W.R., "Heave Force and Pitching Moment on a Submerged Body of Revolution in Finite Depth," MIT Dept. Ocean Eng. Report 70-7 (1970).

angles of deflection and 15 degrees for negative angles of deflection. The results imply that the fin-body interference effect may be expected to be linear up to ± 15 degrees of deflection of an aft fin of low aspect ratio for SWATH ships similar to SWATH 6A.

The lift-curve slope (per radian) obtained by Equation (11b) together with Figure 1 is 2.42 and the experimental value about 2.51. The difference is less than 4 percent of the theoretical value, which is quite satisfactory for an engineering approximation.

Figure 9 shows the experimentally obtained heave and pitch added mass and damping coefficients versus frequency of oscillation for the bare hull and two fin-body combinations. Experimental data were analyzed according to Equations (28), (29), and (33) to (38). The contribution by the x-component forces to the pitch moments were subtracted by taking ℓ_D to be the vertical distance from the main hull axis to the X-gage position which was 72.15 cm. The bar signs indicate the dimensionless quantities. Table 1 gives the dividing factors to nondimensionalized A_{ij} and B_{ij} for i,j = 3 and 5 and $\bar{\omega}$ is defined as $\bar{\omega} = \omega\sqrt{L/g}$.

Figure 9 shows the speed and frequency effects on hydrodynamic coefficients A_{ij} and B_{ij}. Although Equation (3) indicates no speed effect on A_{33}, the experimental results shown in the upper part of Figure 9a reveal some of this effect on A_{33} even for the bare hull, expecially at F_n = 0.384. The effect of frequency on A_{33} appears to be less pronounced than for conventional monohull ships.

Equation (7) predicts that forward speed will strongly affect A_{55}, and this is confirmed experimentally; see the lower part of Figure 9a. According

to Equation (7), speed and frequency effects are represented by U^2/ω^2. The experimental results appear to confirm this in the lower frequency region.

Figure 10 presents the heave and pitch damping coefficients B_{33} and B_{55}. For the bare hull (Figure 10a) the speed-dependent term in the expression of B_{33} in Equation (4) is $\rho a_0 U \int_L B_m \, dx$. This implies that an increase in B_{33} from the zero-speed values is expected to be proportional to the speed. According to Equation (8), the increase in B_{55} from the zero-speed values for the bare hull is contributed by

$$\frac{U^2}{\omega^2} \int_L b_{33} \, dx + \rho a_0 U \int_L x^2 B_m \, dx$$

Figure 10a exhibits the expected trends although they are not as clear for B_{55} as for B_{33}, because of the scaling of the graphs. As expected from Equations (4) and (8), the addition of fins to the bare hull significantly increases the damping coefficients. To check the accuracy of the prediction of speed effects, the speed ratio obtained by $\frac{0.538}{0.384} = 1.4$ can be compared to ratio obtained by

$$\frac{(B_{33})_{0.538} - (B_{33})_0}{(B_{33})_{0.384} - (B_{33})_0}$$

where the subscripts indicate the Froude numbers. Bare hull (Figure 10a), Aft Fin A (Figure 10b) and both fins (Figure 10c) all give the values between 1.3 and 1.5 for this ratio; this demonstrates that the speed effect on B_{33} is satisfactorily represented by Equation (4). It is interesting to note that frequency has very little effect on B_{55}.

The coupled added mass coefficients are shown in Figure 11. As would be

expected from Equation (5), the speed effect is significant for A_{35} because of the fin effect. The coupled damping coefficients are shown in Figure 12; note that the values of B_{35} and B_{53} are close to zero at zero speed for all three hull conditions. One can see, from Equations (6) and (10), that one of the speed-dependent terms UA_{33} is additive for B_{35} and subtractive for B_{53}; this effect can easily be observed in Figure 12.

Figures 13 to 18 compare theoretical and experimental values of the hydrodynamic coefficients associated with heave-pitch motion.

The values of A_{33} and A_{55} for three SWATH 6A configurations at $F_n = 0$ are shown in Figure 13. The mass $m_i^{(f)}$ (when the data is not given) and the heave added mass $a_{33i}^{(f)}$ of the fins were estimated in the theory by

$$m_i^{(f)} = \rho \frac{\pi}{4} t_i c_i s_i$$

where t_i, c_i, and s_i are respectively the average thickness, chord, and span of the ith fin, and

$$a_{33i}^{(f)} = \rho \frac{\pi}{4} c_i^2 s_i$$

In other words, the mass of fin is assumed to be the same as the displaced water mass of a fin with elliptical foil sections, and $a_{33i}^{(f)}$ is the same as the water mass displaced by a circular cylinder which has a diameter equal to the chord of the fin and a length equal to the span.

The following values were used for the theoretical results; see Equations (3) to (10):

$$a_0 = 0.07$$

$$\int_L B_m \, dx = 5.71 \times 10^{-2} L^2$$

$$-\int_L x B_m \, dx = 4.15 \times 10^{-4} L^3$$

$$\int_L x^2 B_m \, dx = 4.11 \times 10^{-3} L^4$$

The projected areas of the forward and aft fins were respectively

$$A_1^{(f)} = 2 \times 159.1 \ cm^2$$

and

$$A_2^{(f)} = 2 \times 474.5 \ cm^2$$

and the location of the fins were

$$\ell_1 = 81.4 \ cm$$

and

$$\ell_2 = -119 \ cm$$

Considerable discrepancies can be noticed between the experimental and theoretical results for A_{33}. Similar plots for the other two speeds are shown in Figures 13b and 13c. Although, according to the theory, speed has no effect on A_{33}, the experimental results have indicated some speed effects but they are not significant. It can be observed from Figures 13a to 13c that the discrepancy between thecry and experiment is almost a constant value over the frequency range shown. The constant appears to be greater for the finned bodies. At F_n = 0.384, experimental

values for A_{33} are about 20 to 30 percent higher for finned bodies than for the bare hulls, as shown in Figure 13b. No satisfactory explanation can be offered at this time for such a large effect of small fins on A_{33}. In the average, the theoretical values of A_{33} and A_{55} are about 10 to 15 percent less than the experimental values. This demonstrates the case that the strip approximation does not necessarily always overestimate the values of A_{33} and A_{55}. The large experimental values of A_{55} at the lower frequencies at $F_n = 0.538$ confirm the effect of the term $\frac{U^2}{\omega 2} A_{33}$ in Equation (7). The better agreement between the two results for A_{55} at $F_n = 0.538$ is considered to be due to the dominant magnitude of $\frac{U^2}{\omega 2} A_{33}$ over other terms in Equation (7).

To be compatible with the theoretically obtained added mass coefficients, the restoring coefficients C_{ij} used in Equations (28), (33), (35), and (36) should be the values obtained at zero speed except C_{55} which is speed dependent as defined earlier by

$$C_{55} = \rho g \nabla \left(I_w / \nabla - \bar{BG} \right) - \rho U^2 \sum_i A_i^{(f)} \ell_i \, C_{\omega i}$$

(See page 5)

We can obtain the values of C_{55} defined in the above by removing the terms $- U^2 A_{33} - \rho a_0 U^2 \int_L x B_m \, dx$ from Equation (47) as follows:

Since

$$(C_{55})_{\text{Bare hull at } F_n = 0} = \rho g \nabla \left(\frac{I_w}{\nabla} - \bar{BG} \right)$$

and

$$(C_{55})_{\text{Bare hull at } F_n > 0} = \rho g \nabla \left(\frac{I_w}{\nabla} - \bar{BG} \right) - U^2 A_{33} - \rho a_0 U^2 \int_L x B_m \, dx$$

we can easily find that

$$U^2 A_{33} + \rho a_0 U^2 \int_{\ell} x B_m \, dx = (C_{55})_{\text{Bare hull at } F_n = 0} - (C_{55})_{\text{Bare hull at } F_n > 0}$$

Thus, we find that at each Froude Number F_n, the values of C_{55} can be obtained by

$$(C_{55})_{F_n} = [(C_{55}')_{F_n} \text{ in Table 9} + (C_{55}')_{F_n=0} \text{ of bare hull in Table 9} - (C_{55}')_{F_n>0} \text{ of bare hull in Table 9}] \times 180/\pi \text{ (N-m/rad)}$$

Table 11 shows the value of C_{55} used in Equation (36).

TABLE 11

VALUE OF C_{55} USED IN EQUATION (36) TO OBTAIN EXPERIMENTAL VALUES OF A_{55}

Hull Condition	F_n	C_{55} N-m/rad
Bare Hull	0	751.5
	0.384	751.5
	0.538	751.5
With Aft Fin A	0	751.5
	0.384	1471.9
	0.538	2652.8
With Foreward Fin and Aft Fin A	0	751.5
	0.384	1347.6
	0.538	2302.7

The values of B_{33} and B_{55} are shown in Figure 14 for three configurations and speeds. The peak amplitudes of heave and pitch motion are most sensitive to these coefficients. The inherently small heave and pitch damping was significantly augmented by the fins. Thus, success in reliably predicting the motions of SWATH ships with fins depends largely on the accuracy with which the damping coefficients contributed by the fins can be predicted. It can be observed from theoretical expressions for B_{33} and B_{55} (given in Equations (4) and (8)) that fin-contributed damping is dependent on the lift-curve slope $C_{L\alpha}$. Due to the wide scatter in experimental values of $C_{L\alpha}$ obtained from the static tests (Table 10), the theoretical values obtained by Equations (11) to (13) and shown in Table 10 were used to evaluate B_{33} and B_{55} in Equations (4) and (8), respectively. Good agreement between experiment and theory was obtained by using the aforesaid theoretical values of $C_{L\alpha}$, as shown in Figures 14a to 14c. Predicted heave and pitch motion of SWATH 6A based on these damping coefficients correlated well with the model experimental results.[1]

Agreement between theoretical and experimental values of A_{35} and A_{53} (Figure 15) was good except for A_{53} at $F_n = 0.538$ (Figure 15c). One can see from Equation (35) that C_{53} is involved in obtaining the experimental value of A_{53}. The value of C_{53} at $F_n = 0.538$ as well as that for C_{35} shown in Table 9 changed significantly from the values at other speeds. Recall that the values of C_{35} and C_{53} used in obtaining A_{35} and A_{53} were those of the bare hull at zero speed. Thus, it can be judged that the sudden opposite trend exhibited for the experimental values of A_{53} at $F_n = 0.538$ must be related to the change in C_{53} at that speed. However, even though a large increase in C_{35} at $F_n = 0.538$ is observed (see Table 9), agreement between the experimental and theoretical results for A_{35} is excellent as can be seen in Figures 15a to 15c. One source of the discrepancy for A_{53} may be an inaccurate estimate of the vertical moment arm

ℓ_D (see Equation (35)) used to subtract the pitch moment contributed by the x-component forces. Furthermore, it should also be noted that the magnitudes of A_{53} are relatively small compared to those of A_{35}. Hence even small errors in the measurement or in the calculation can amplify the discrepancy. Despite the discrepancy observed for A_{53}, there was good agreement between predicted heave and pitch motion in waves and model experimental results. This implies that the present method of evaluating A_{53} may still be valid and thus that the A_{53} term may not significantly affect the motion prediction after all.

It can be seen from the comparison for the coupled damping coefficients B_{35} and B_{53} (Figure 16) that there is a constant discrepancy between theory and experiment for both coefficients for all hull conditions at speeds other than zero. A careful examination of Equations (6) and (10) reveals that the cause of the discrepancy may be associated with the term $\rho a_o U \int_L x B_m \, dx$ This term was derived from the so-called cross-flow effect, as discussed earlier.[1] The major underlying assumption in deriving this term is that the cross-flow velocity induced by vertical ocsillation of the body while running at a constant speed is the same at each cross section of the body. This assumption, together with the assumption of a constant value of the viscous-lift coefficient a_o at any cross section, may be incorrect. An approximate 40 percent increase in the value of the integral $\left| -\int_L x B_m \, dx \right|$ would bring the theoretical values of B_{35} and B_{53} close to the experimental values in the present case.

The results of the wave-exciting heave force and pitch moment are shown respectively in Figures 17 and 18. λ is the length of the wave and L that of the main hull. There is good agreement between experimental and theoretical values for the heave force amplitudes and phases (Figure 17) but not for the pitch moment amplitudes and phases (Figure 18). The experimental results for

pitch moment are approximately twice the predicted values and show phase angles to be almost constant for all wave lengths. At long waves, the phase angle of the pitch moment would be expected to approach $-\pi/2$. It is difficult to explain these discrepancies at present, but it is conjectured that in the experimental data analysis an error could have been made in subtracting the pitch moment contributed by the x-component forces. If the predicted values were wrong, it would be difficult to explain the good agreement in pitch motion obtained between the theoretical and experimental results.[1]

CONCLUDING REMARKS

The present investigation reveals that in general the theoretical methods of predicting the hydrodynamic coefficients of a SWATH configuration with stabilizing fins are valid for predicting heave and pitch motion in waves.

The following information was obtained from the present investigation:

1. Values of the lift-curve slopes of the stabilizing fins obtained in static tests changed significantly for different speeds indicating the presence of free-surface effects. However, when the theoretical values, which are obtained for steady condition in an unbounded fluid, were used in the evaluation of the hydrodynamic coefficients of the finned bodies in oscillatory motion, good agreement was obtained with the data obtained from the oscillation experiments. The downwash effects of the forward fins on the aft fins tend to reduce the lift on the aft fins but not significantly.

2. The trend of the hydrodynamic coefficient with respect to frequency and speed predicted by the theory are confirmed by the experiment except for A_{53} at $F_n = 0.538$.

3. It appears that the values of the term $\rho a_0 U \int_L x B_m dx$ in the theory should be respectively increased 1.3 and 1.5 times in order to agree with the experimentally obtained values of B_{35} and B_{53}.

4. The theoretical values of wave-excited pitch moment of SWATH configurations should be verified. The forward speed effect for A_{53} at high Froude numbers should be reexamined theoretically, although it does not appear to significantly affect the accuracy of the prediction of motion.

ACKNOWLEDGMENTS

The authors acknowledge the contributions made by the participants in the present experiment and are grateful to their supervisor Ms. Margaret D. Ochi and Dr. Milton Martin for their useful suggestions in refining the present report.

REFERENCES

1. Lee, C.M., "Theoretical Prediction of Motion of Small-Waterplane-Area Twin-Hull (SWATH) Ships in Waves," DTNSRDC Report 76-0046(1976)

2. Pitts, W.C. et al, "Lift and Center of Pressures of Wing-Body-Tail Combinations at Subsonic, Transonic, and Supersonic Speeds," NACA Report 1307 (1959)

3. Whicker, L.F. and L.F. Fehlner, "Free-Stream Characteristics of Family of Low-Aspect-Ratio, All-Movable Control Surfaces for Application to Ship Design," DTMB Report 933 (1958).

4 Lee, C.M., and M. Martin, "Determination of Size of Stabilizing Fins for Small Waterplane Area, Twin-Hull Ships," DTNSRDC Report 4495 (1974)

5 Gertler, M. and G.R. Hagen, "Standard Equations of Motion for Submarine Simulation," DTNSRDC Report 2510 (1967)

6 Korvin-Kroukovsky, B.V. et al, "Theoretical and Experimental Investigation of the Interaction of a Free Surface and a Body of Revolution Moving under It," Experimental Towing Tank, Stevens Inst. Tech Report 390 (1950).

7 McCreight, W.R., "Heave Force and Pitching Moment on a Submerged Body of Revolution in Finite Depth," MIT Dept. Ocean Eng. Report 70-7(1970).

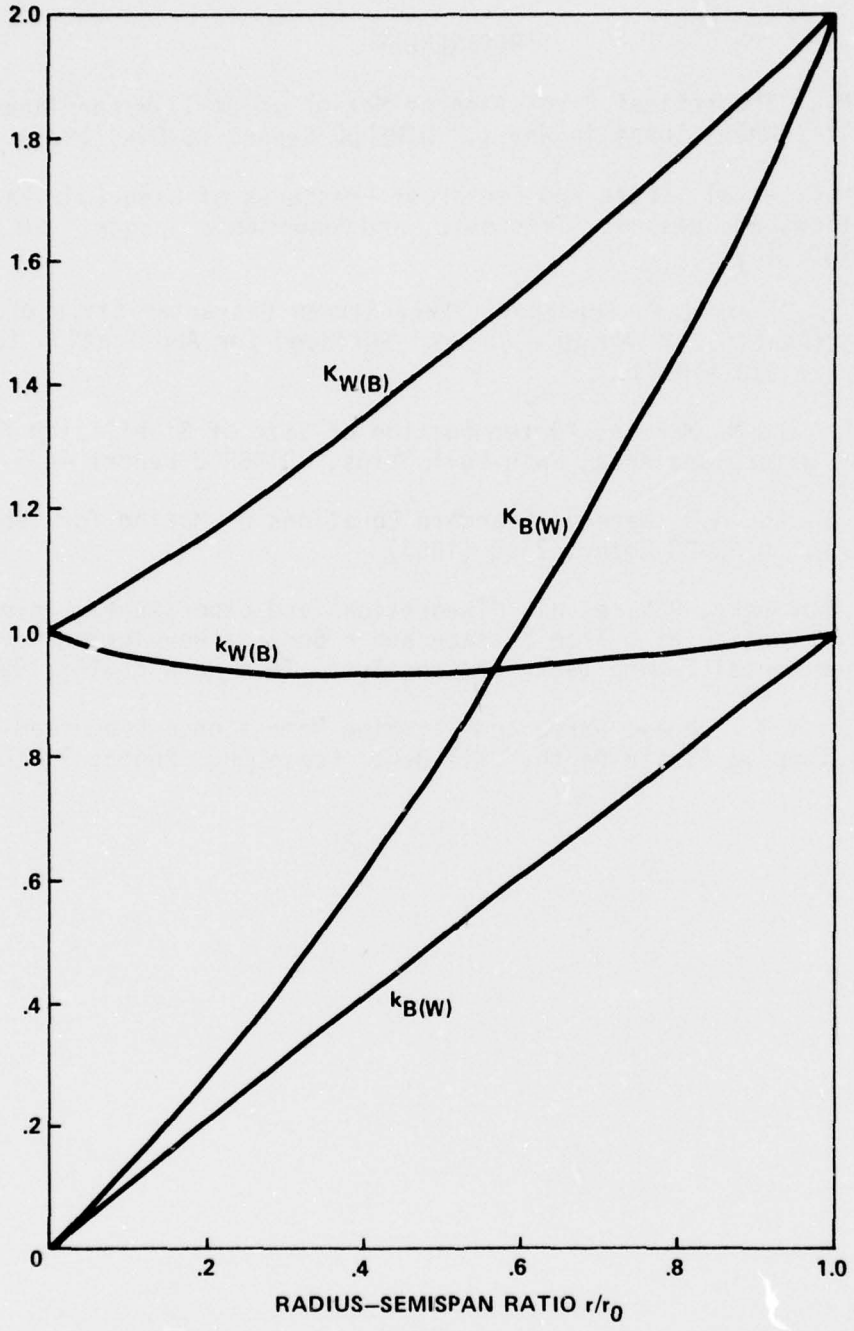

Figure 1 - Values of Lift Ratios Based on Slender-Body Theory
(From Pitts et al.[2])

Figure 2 - SWATH 6A Model and Experimental Setup

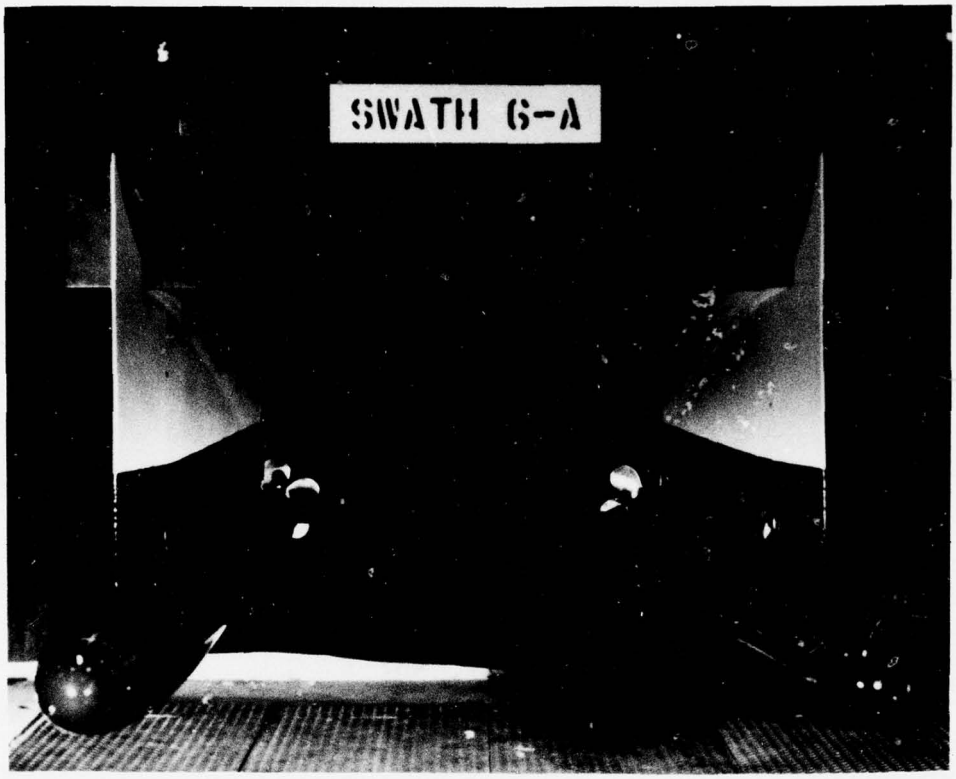

Figure 2a - Bow View

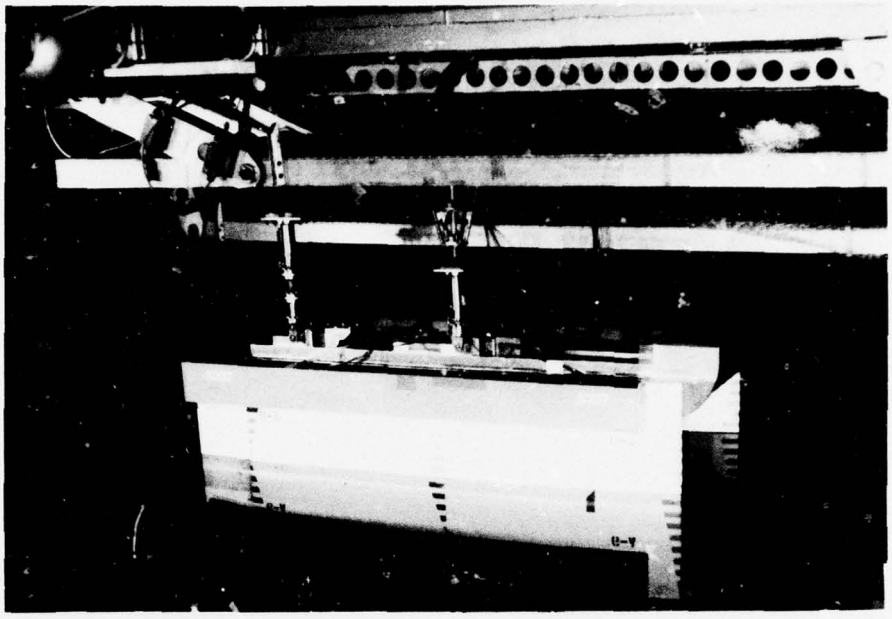

Figure 2b - Setup for Pitch Oscillation

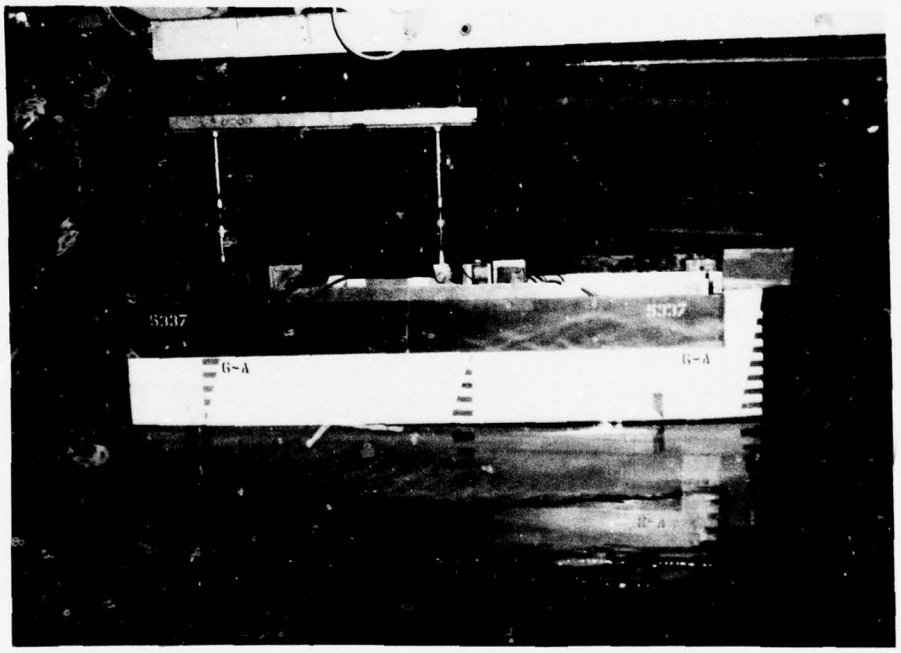

Figure 2c - Setup for Heave Oscillation

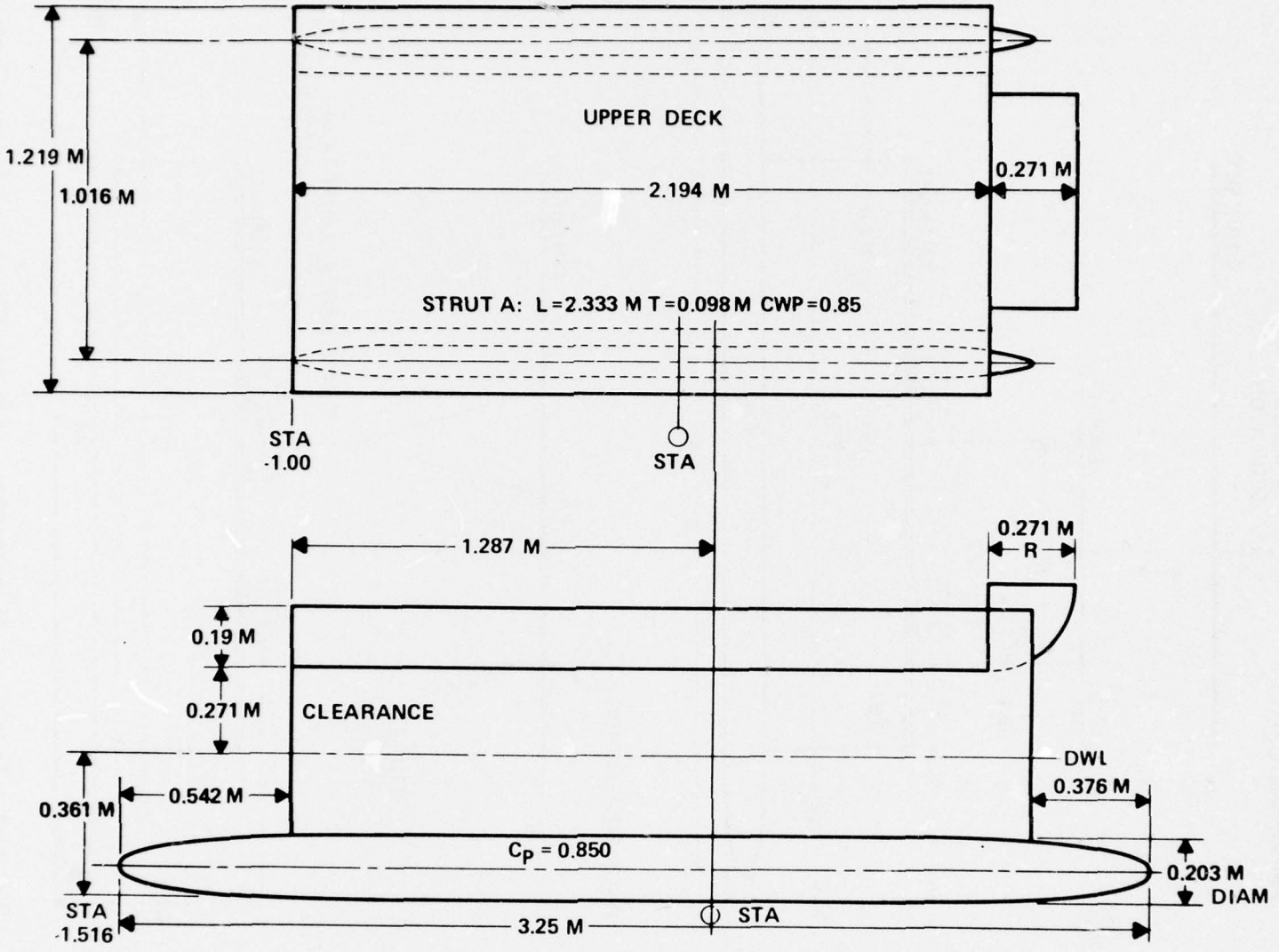

Figure 3 - Top and Side Views of SWATH 6A Model

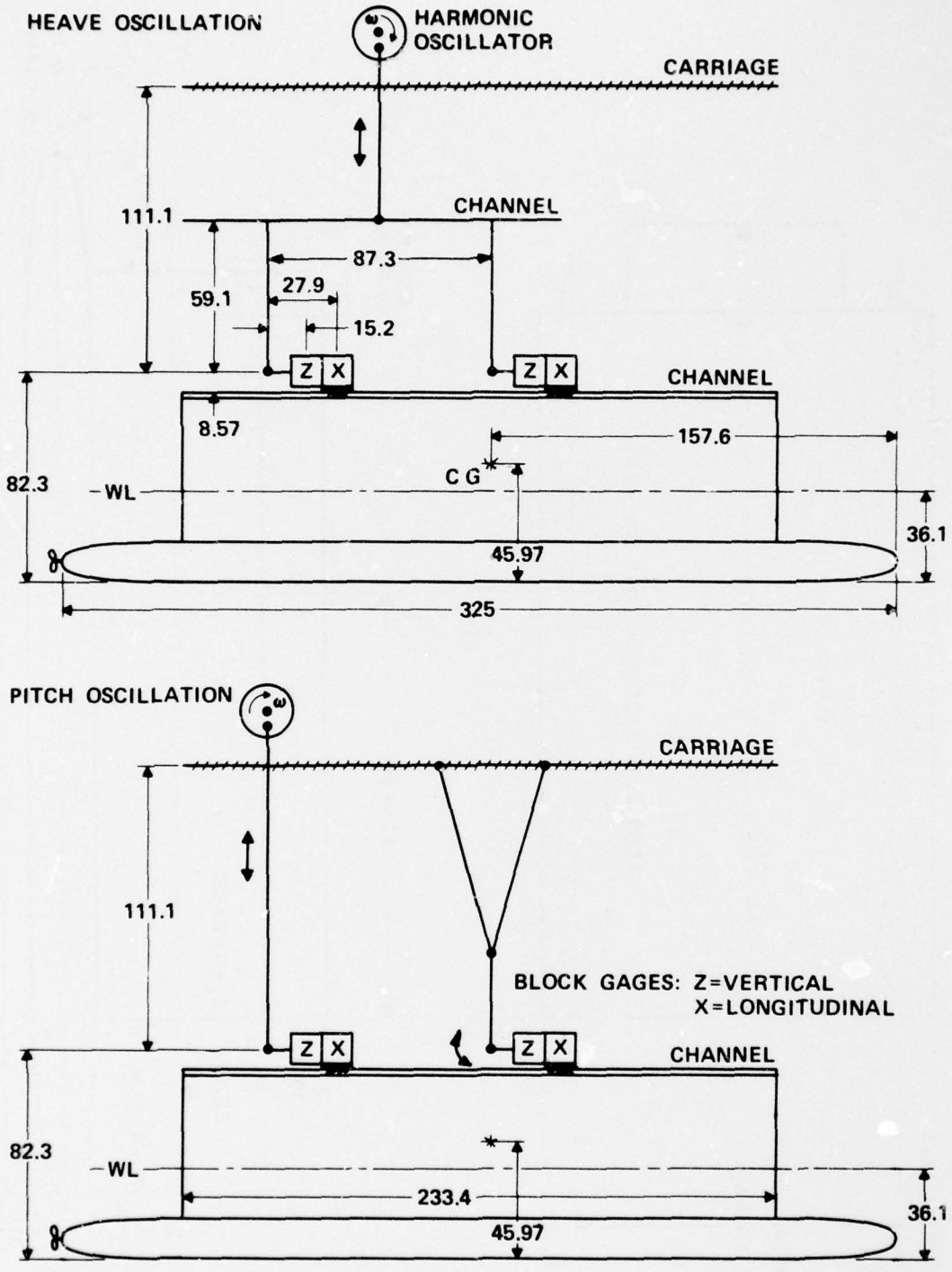

Figure 4 - Details of Experimental Setup for Forced Oscillation Tests
(Lengths are in centimeters)

Figure 5 - Pitch Moment and Vertical Force versus Trim Angle for Various Configurations of SWATH 6A

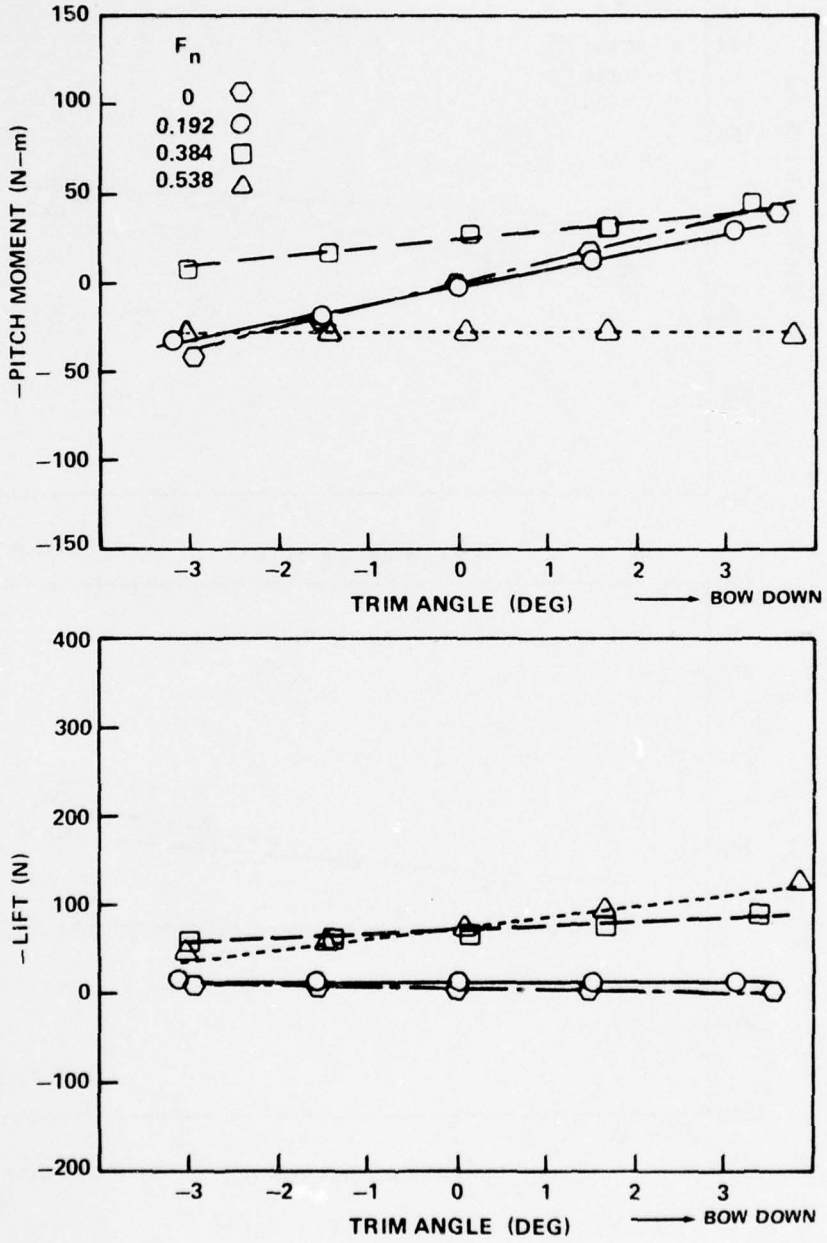

Figure 5a - Bare Hull

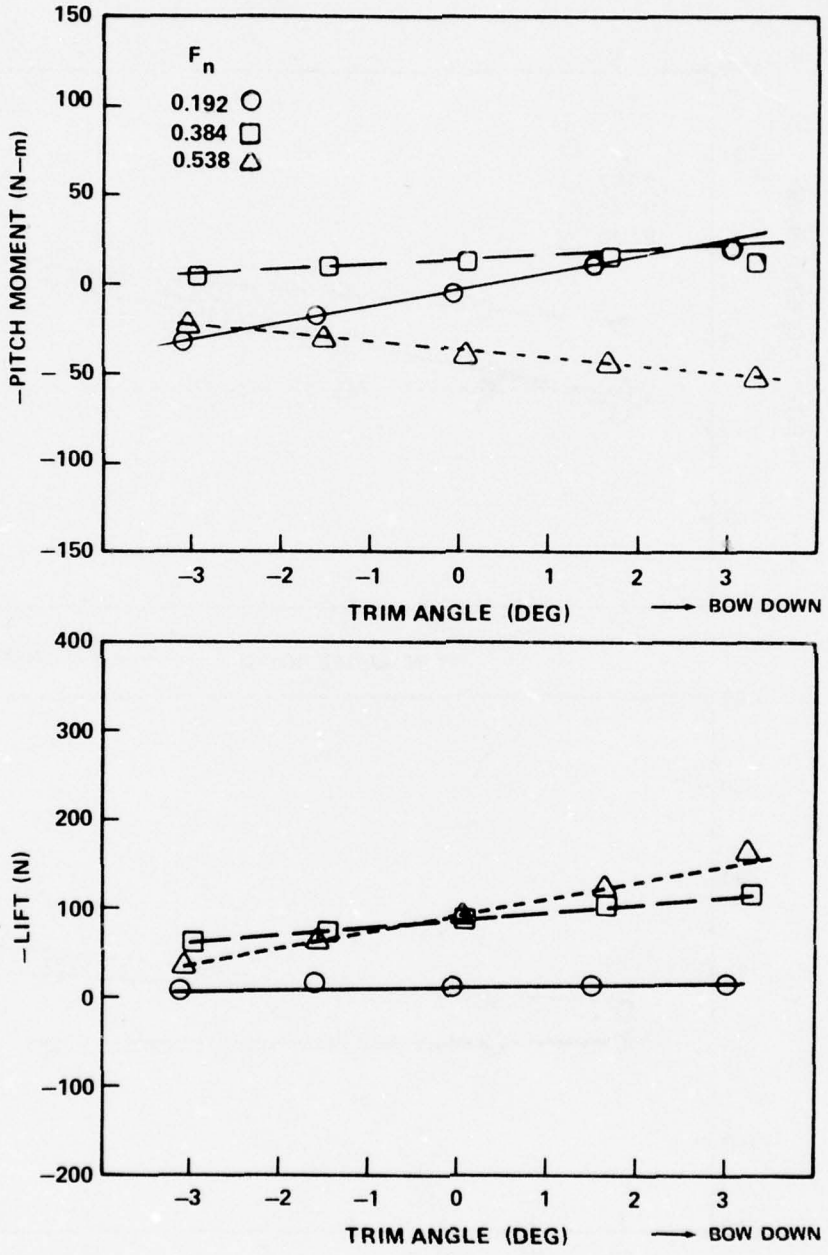

Figure 5b - With Forward Fin

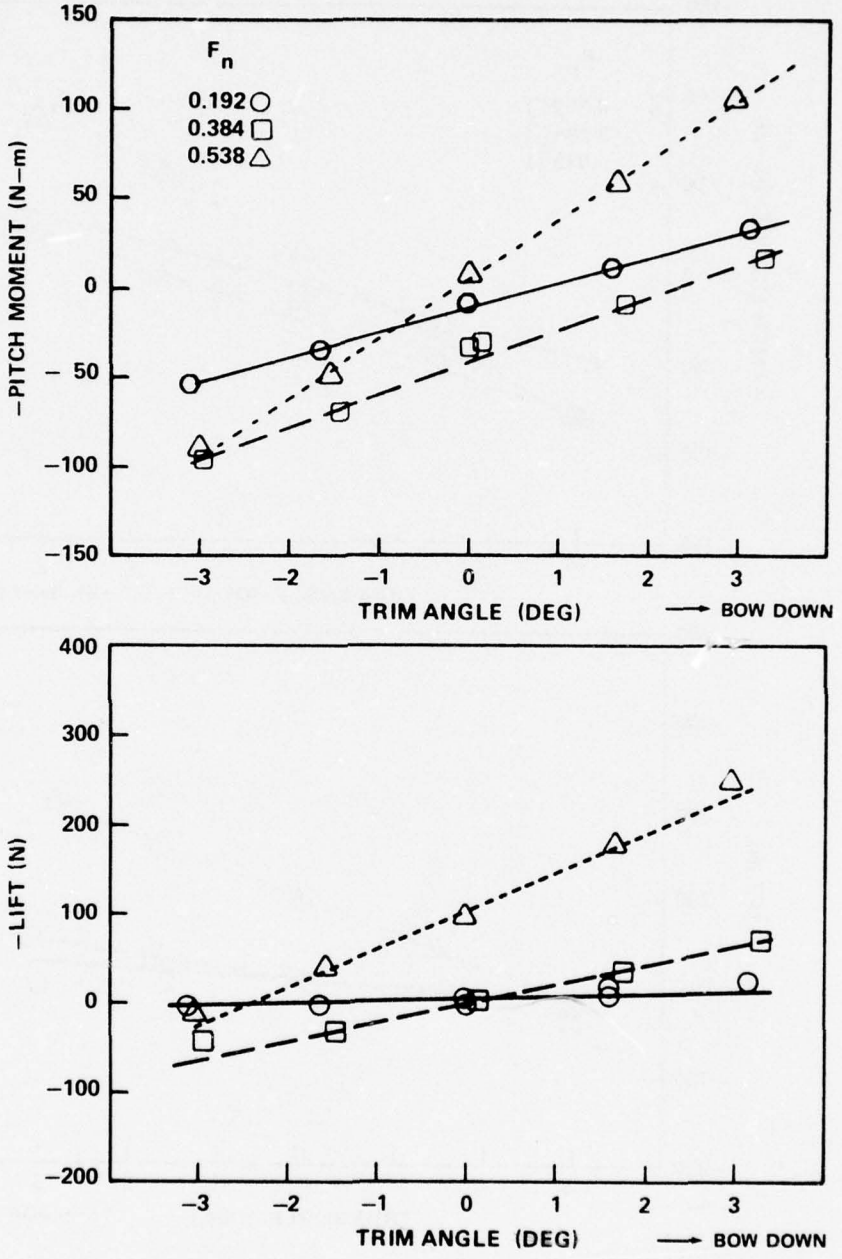

Figure 5c - With Aft Fin A

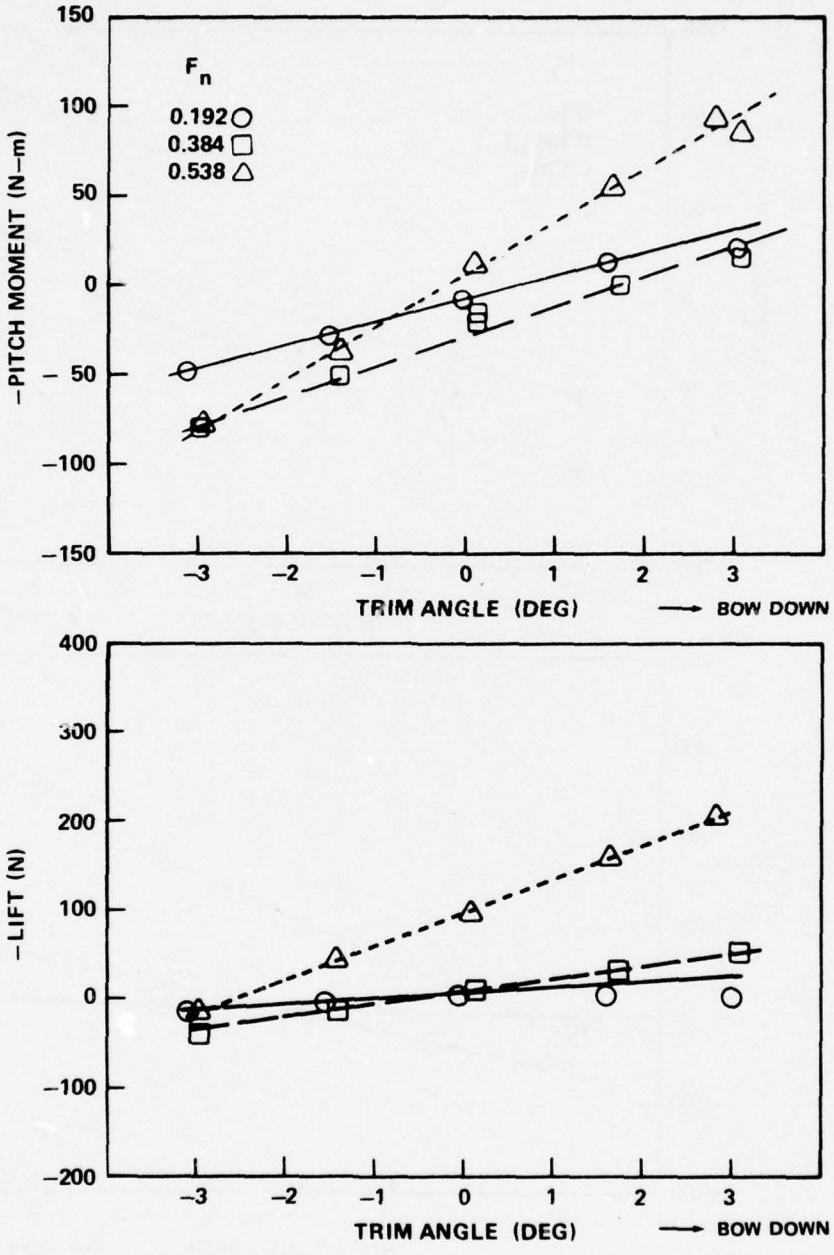

Figure 5d - With Aft Fin B

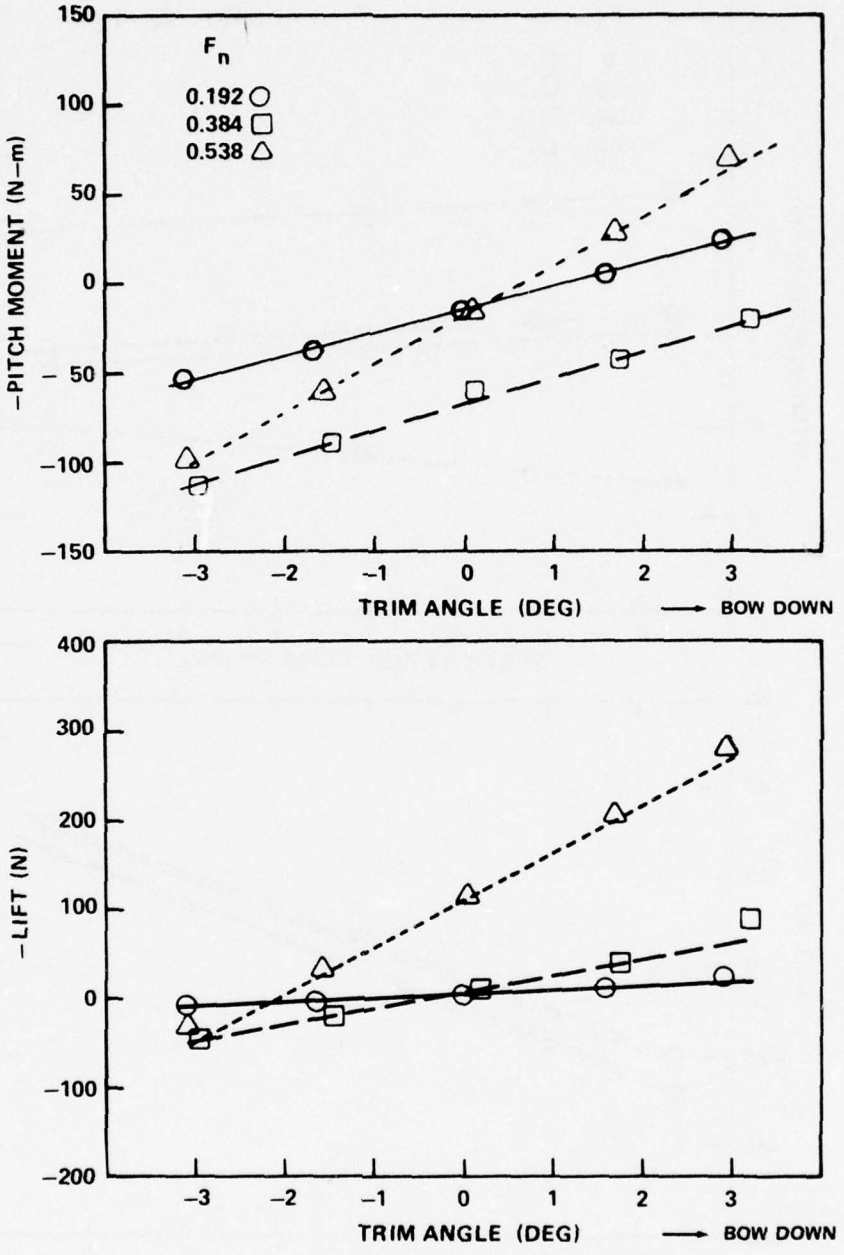

Figure 5e - With Forward Fin and Aft Fin A

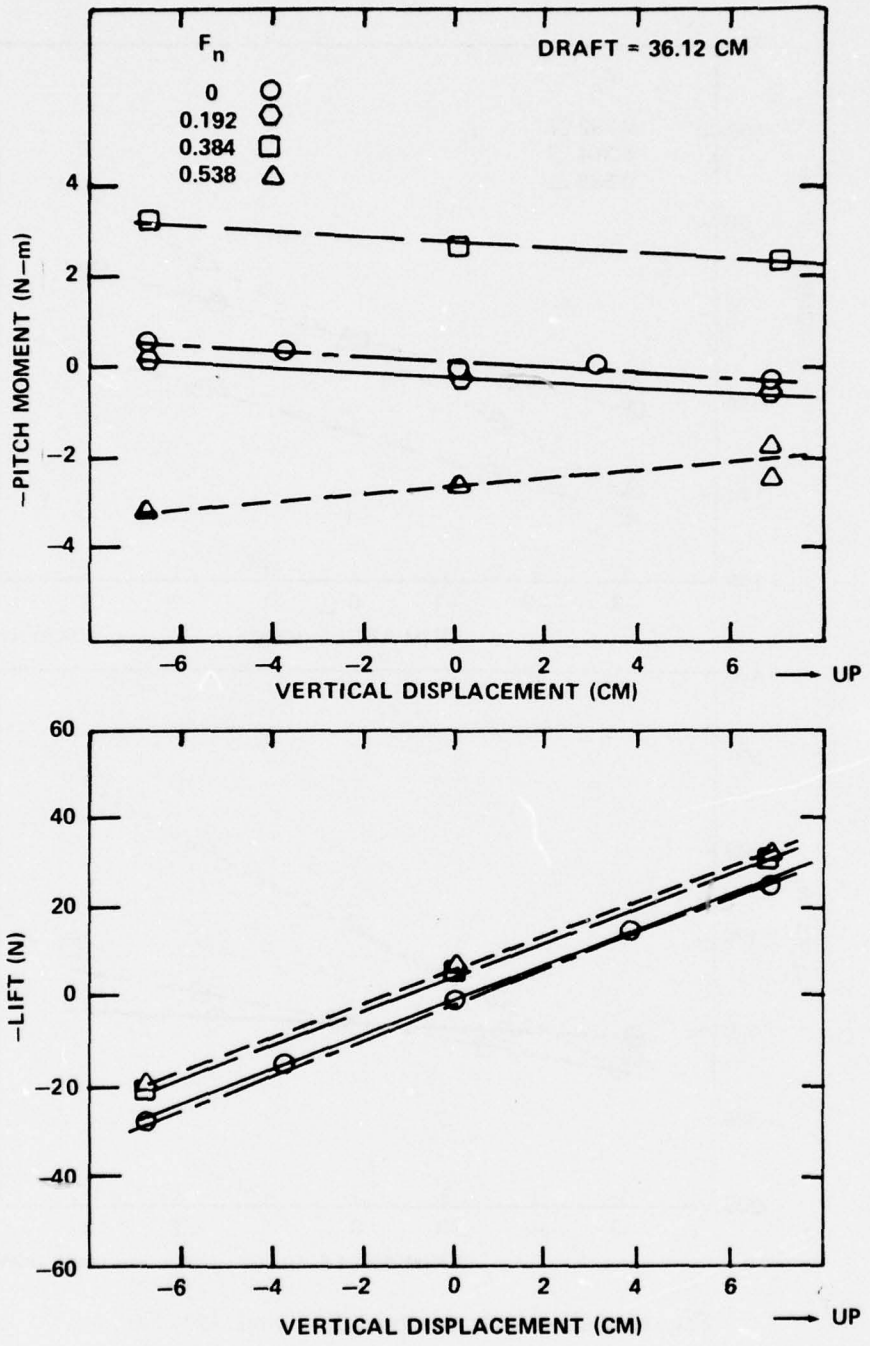

Figure 6 - Pitch Moment and Vertical Force versus Draft for SWATH 6A Bare Hull at Various Speeds

Figure 7 - Pitch Moment and Vertical Force versus Trim Angle for SWATH 6A at Various Speeds

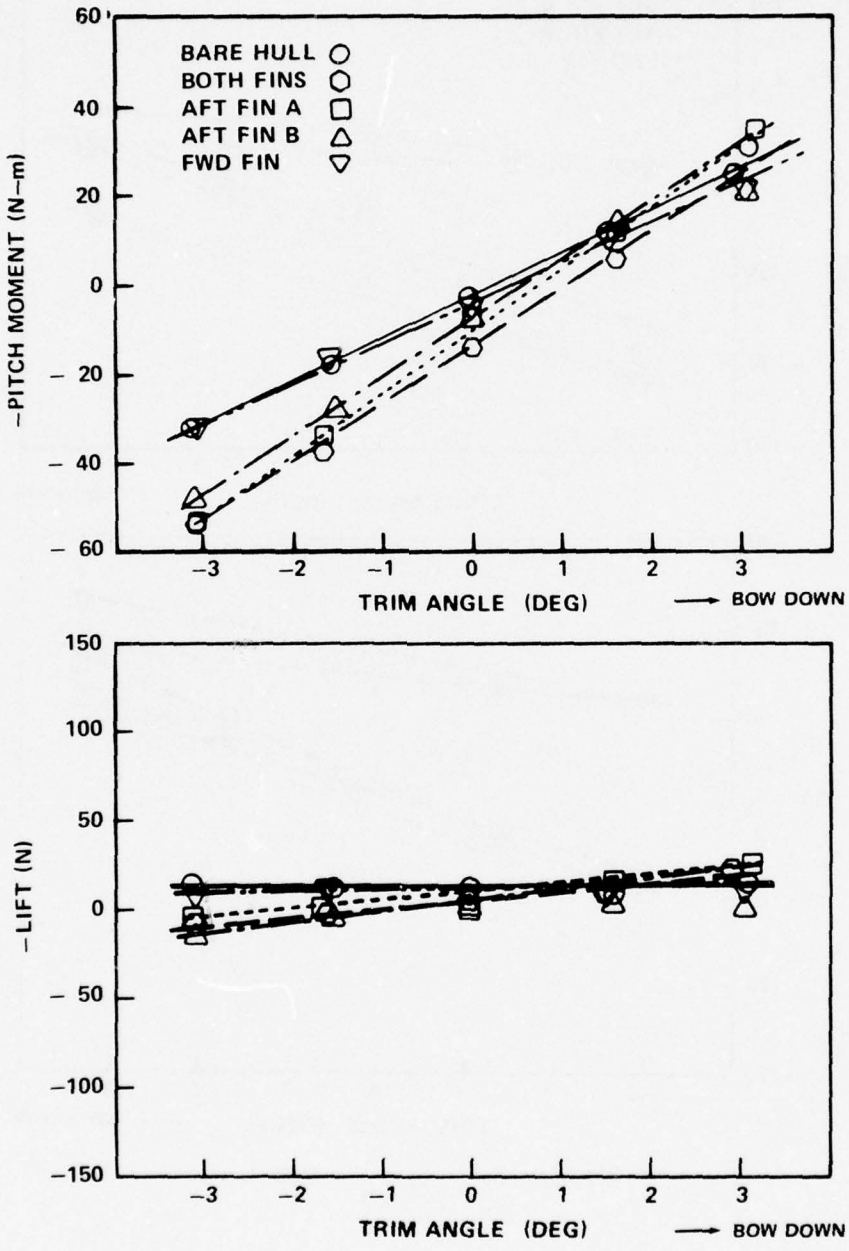

Figure 7a - At F_n = 0.192

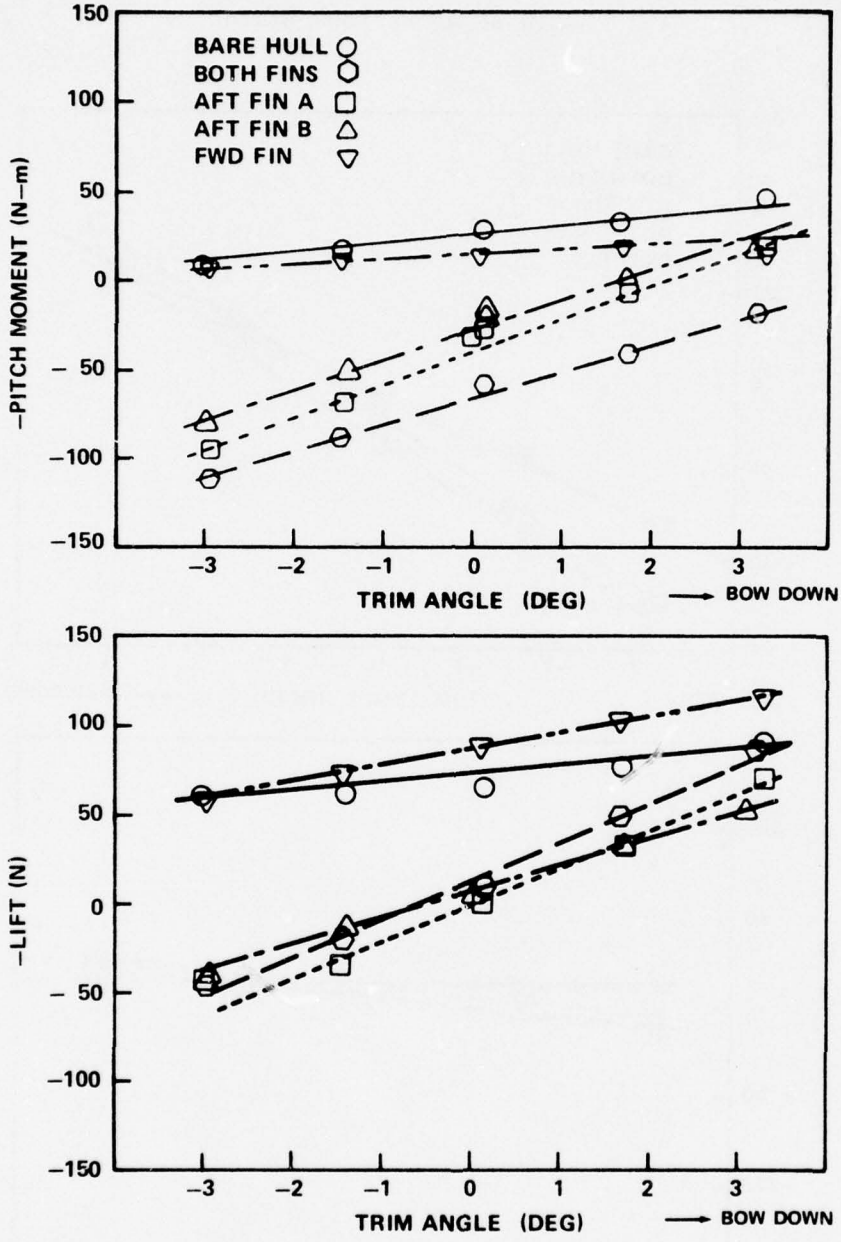

Figure 7b - At F_n = 0.384

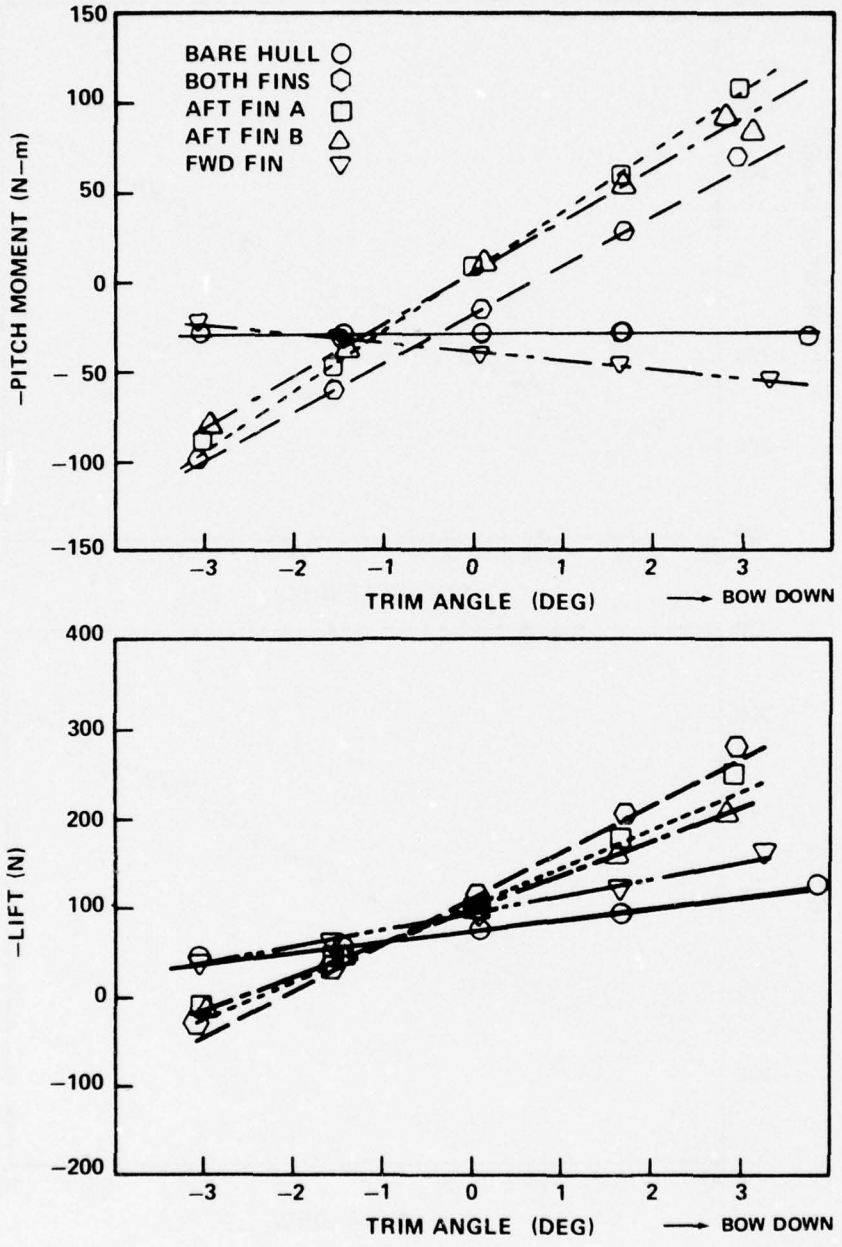

Figure 7c - At F_n = 0.538

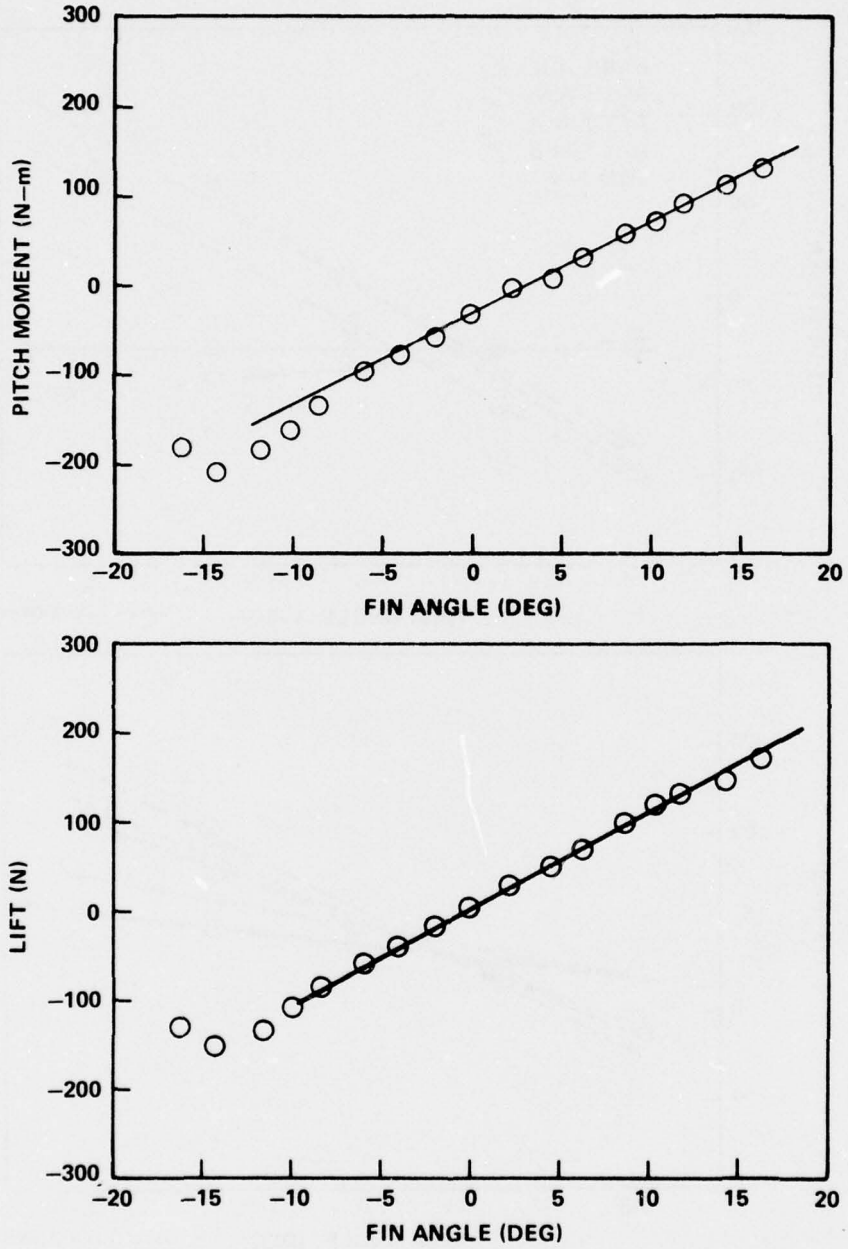

Figure 8 - Effect of Deflection Angle of Aft Fin A on Pitch Moment and Vertical Force of SWATH 6A at F_n = 0.384

Figure 9 - Heave and Pitch Added Mass Coefficients versus Frequency for SWATH 6A

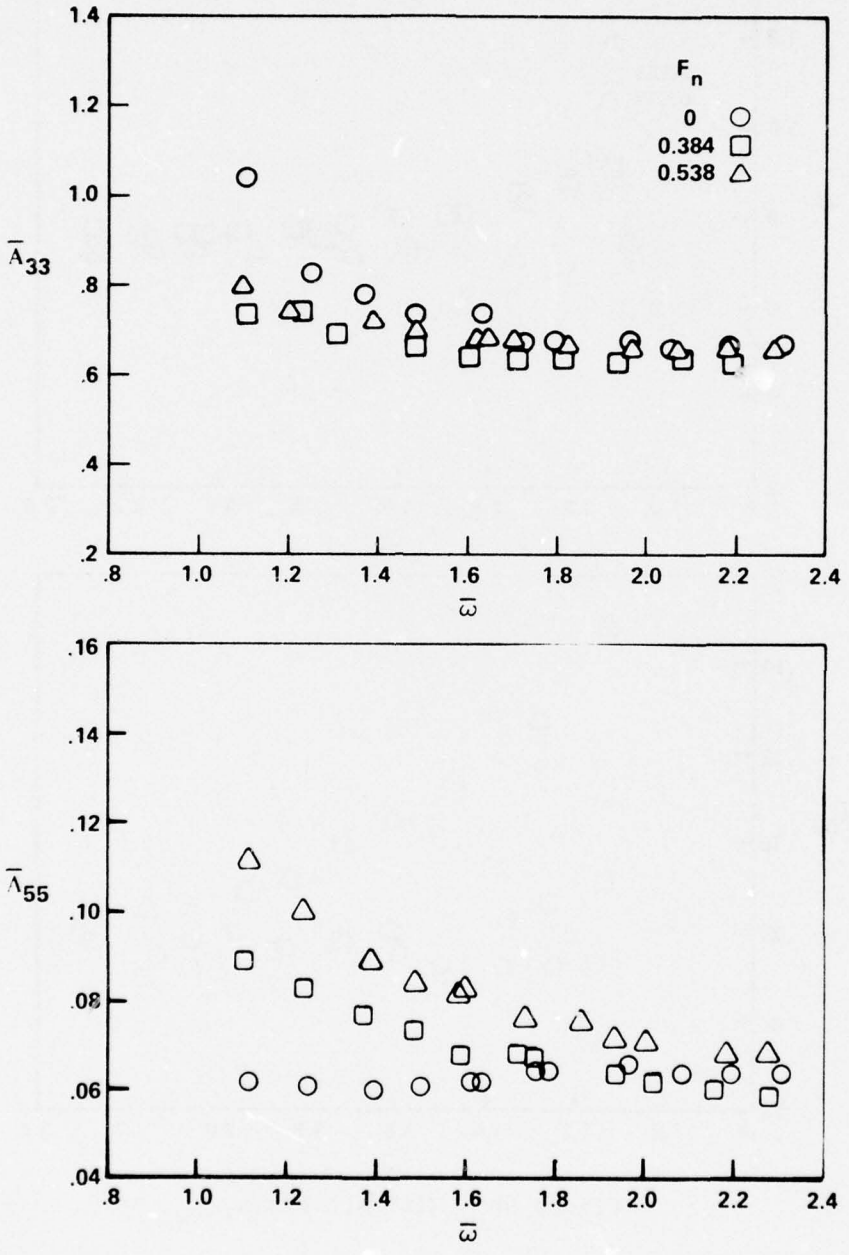

Figure 9a - Bare Hull

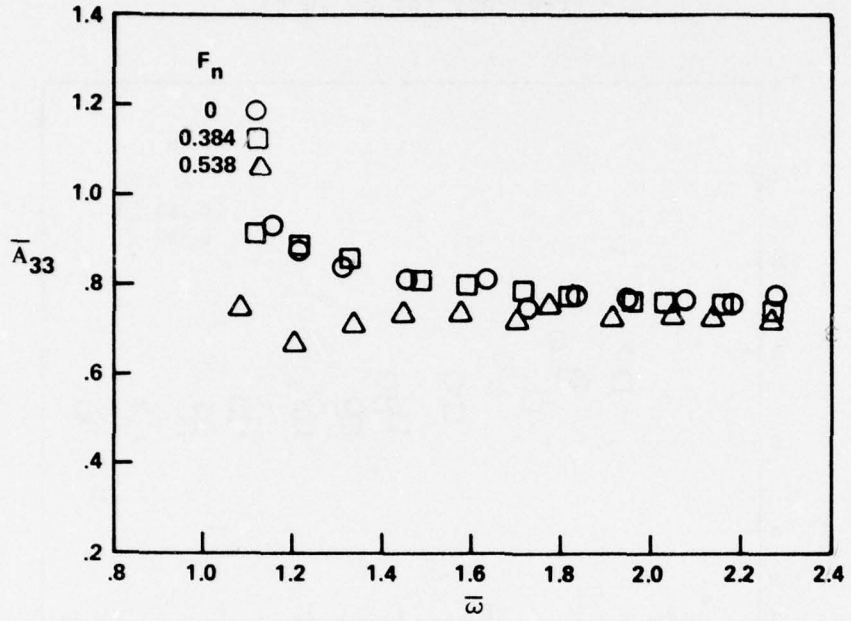

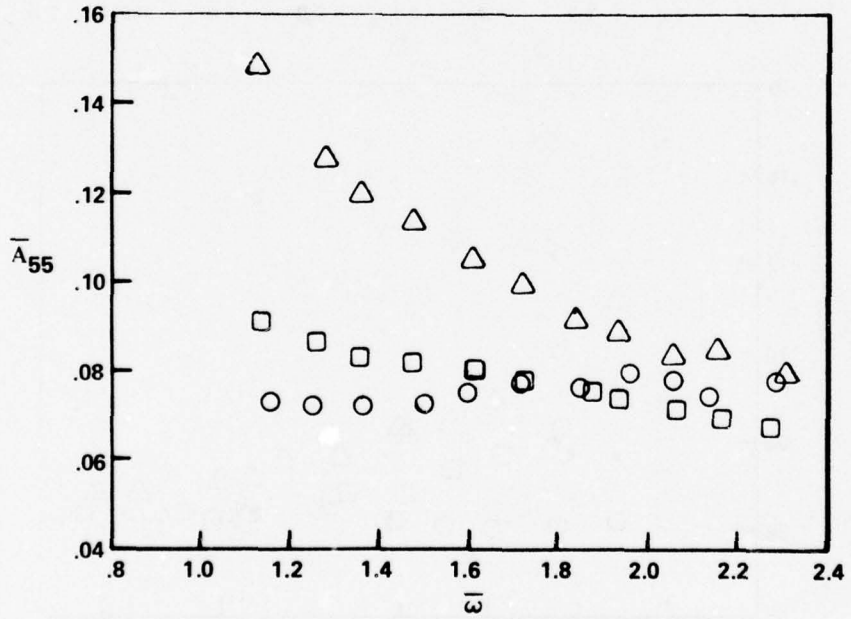

Figure 9b - With Aft Fin A

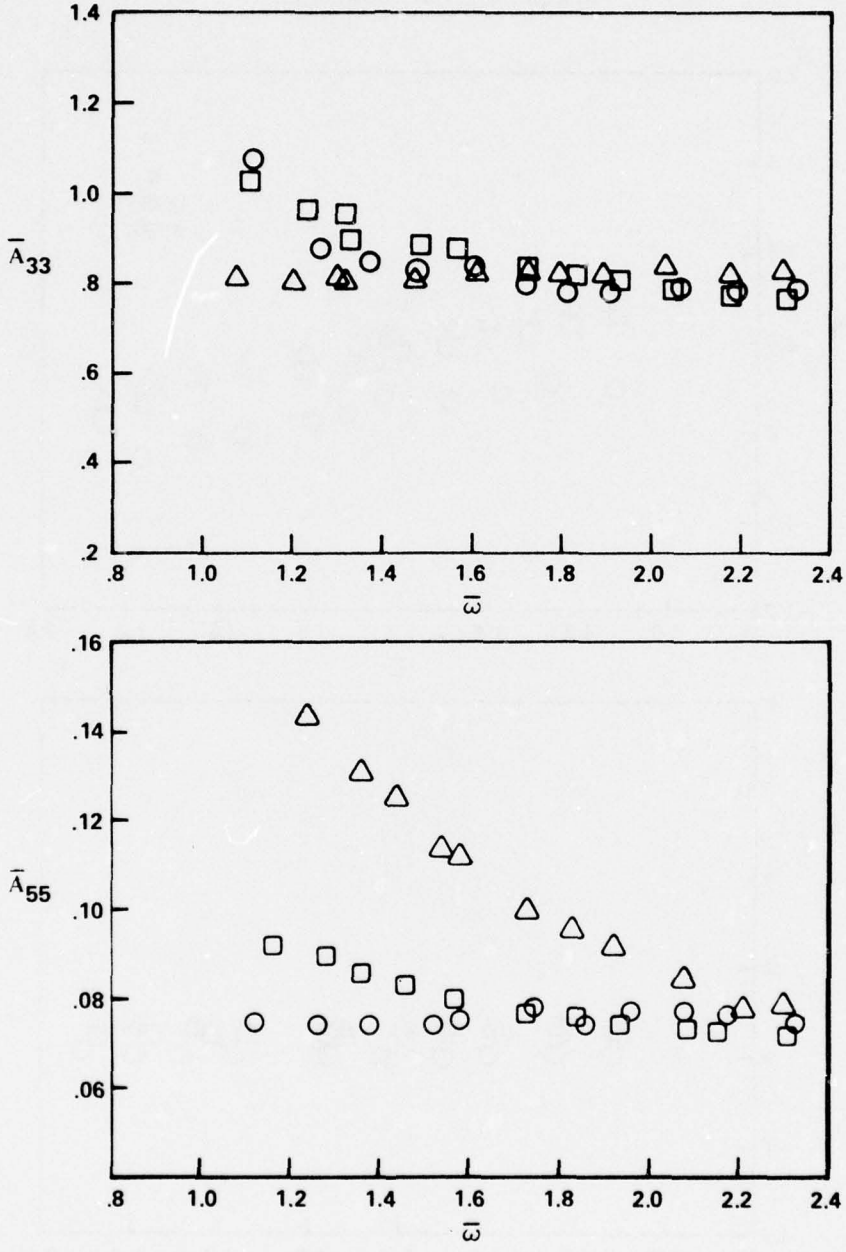

Figure 9c - With Forward Fin and Aft Fin A

Figure 10 - Heave and Pitch Damping Coefficients versus Frequency for SWATH 6A

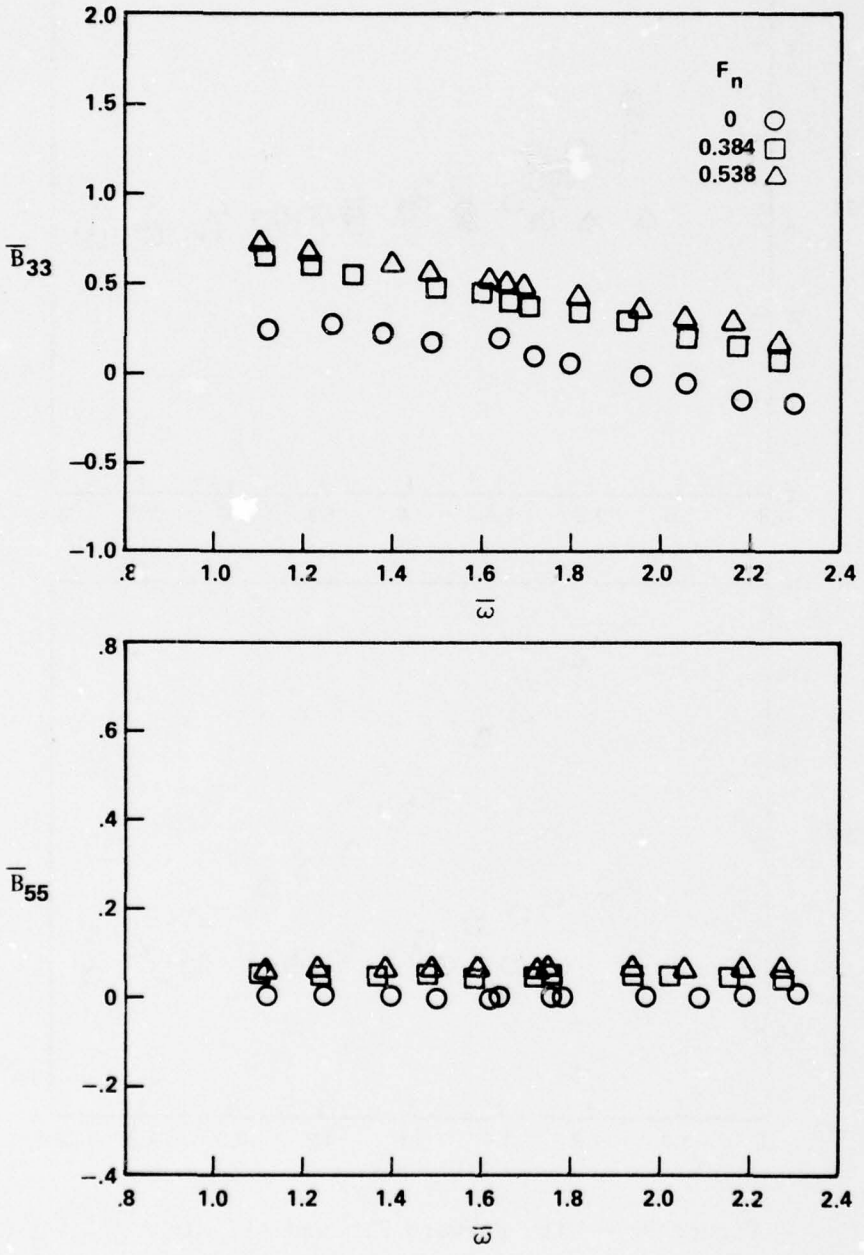

Figure 10a - Bare Hull

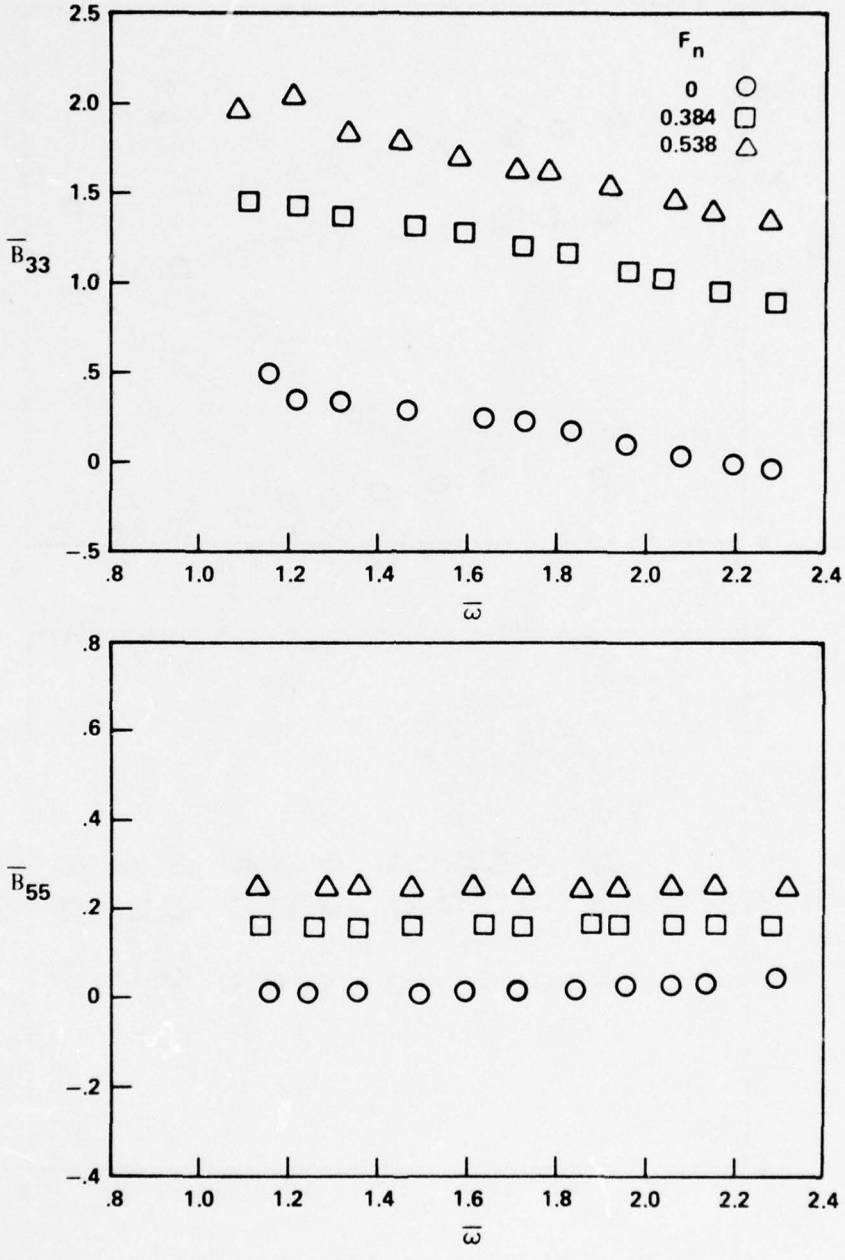

Figure 10b - With Aft Fin A

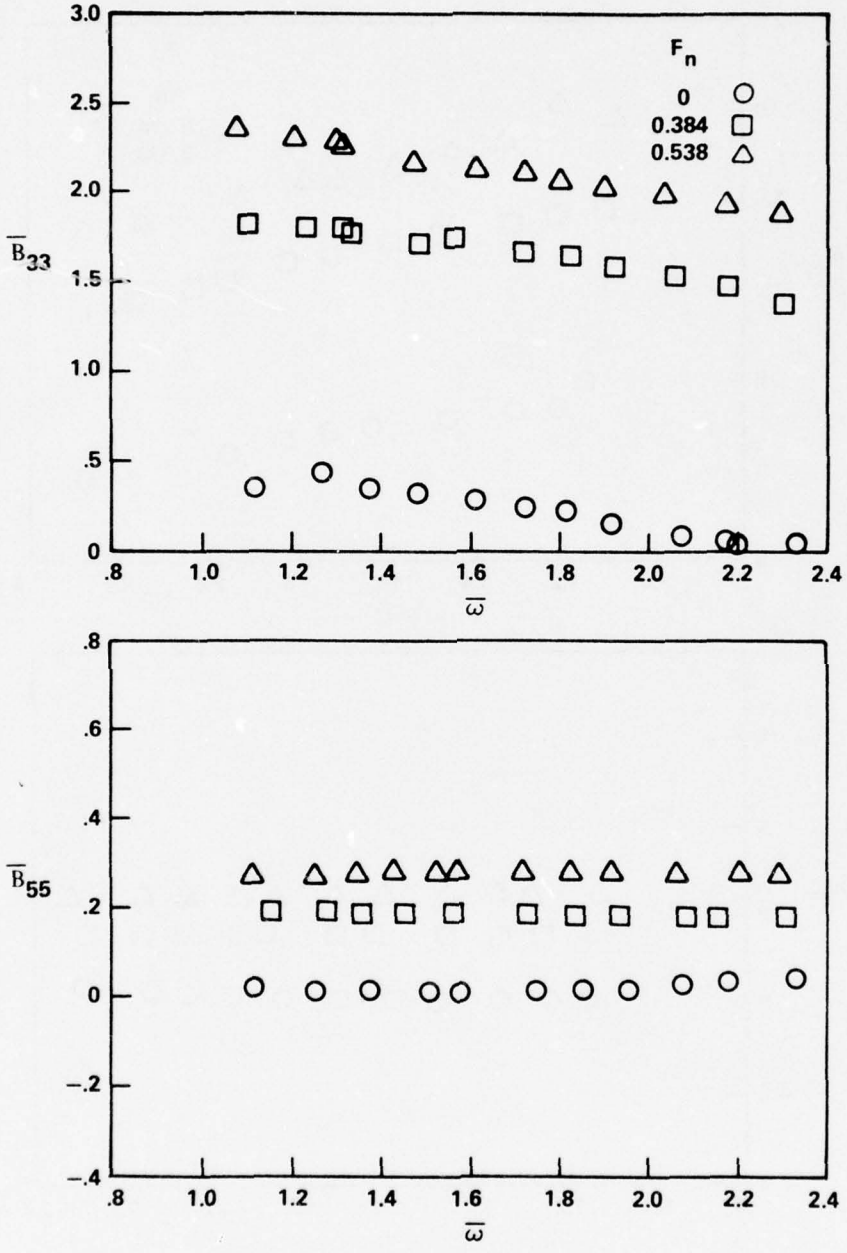

Figure 10c - With Forward Fin and Aft Fin A

Figure 11 - Heave-Pitch Coupling Added Mass Coefficients versus Frequency for SWATH 6A

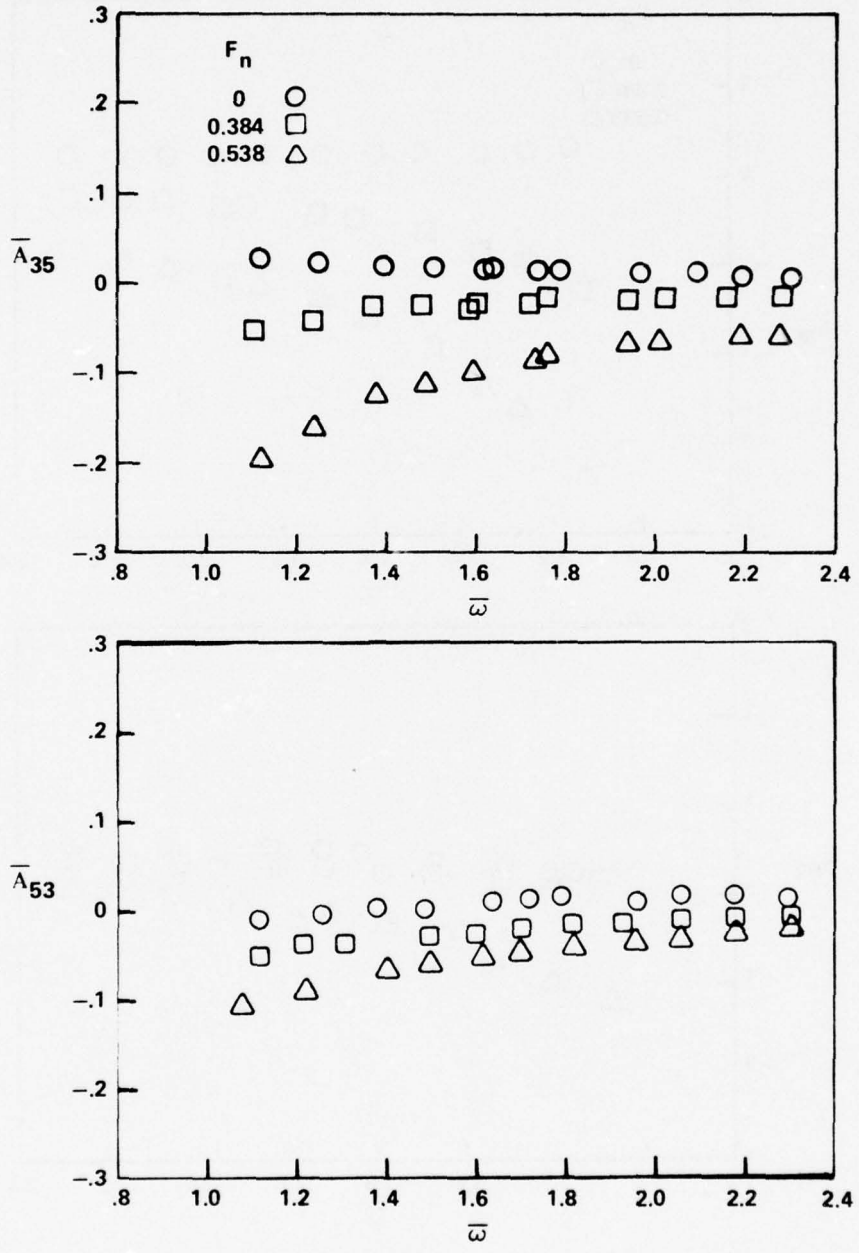

Figure 11a - Bare Hull

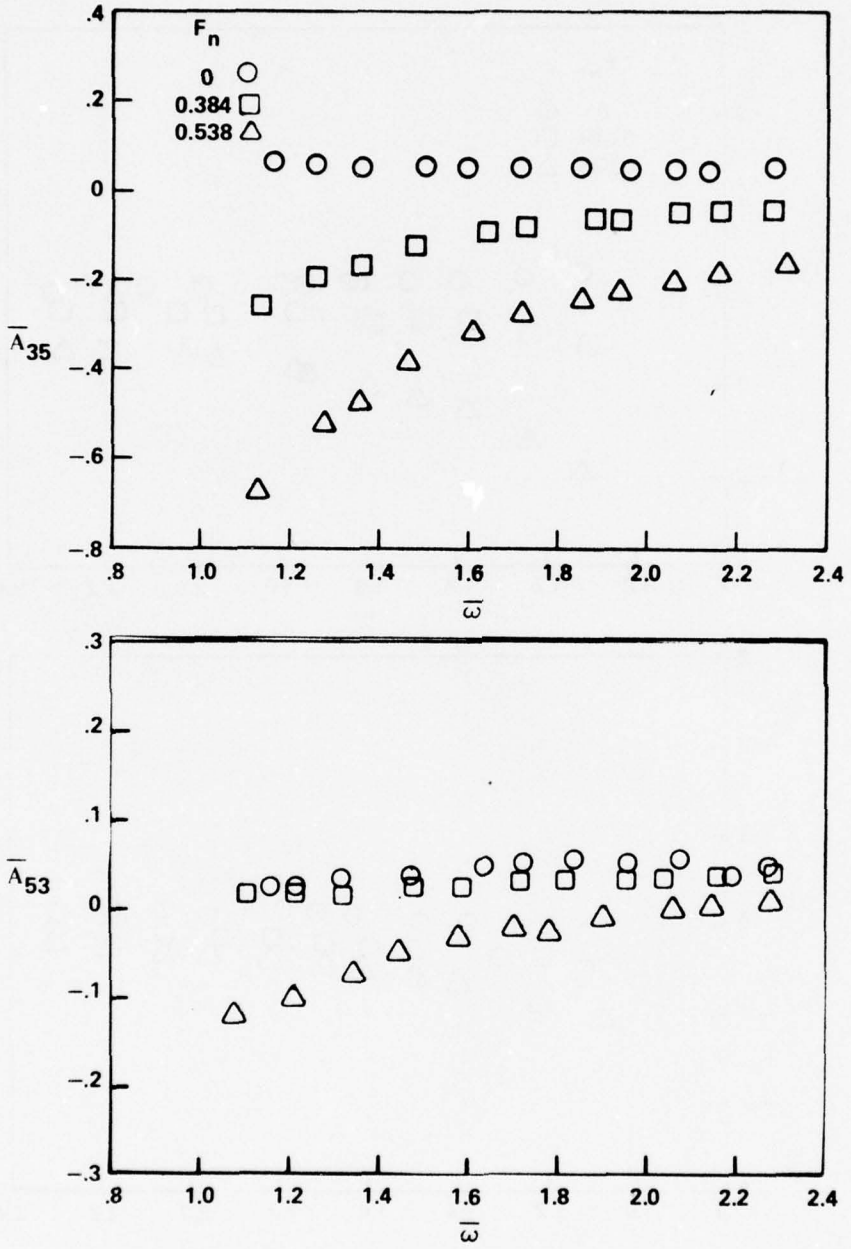

Figure 11b - With Aft Fin A

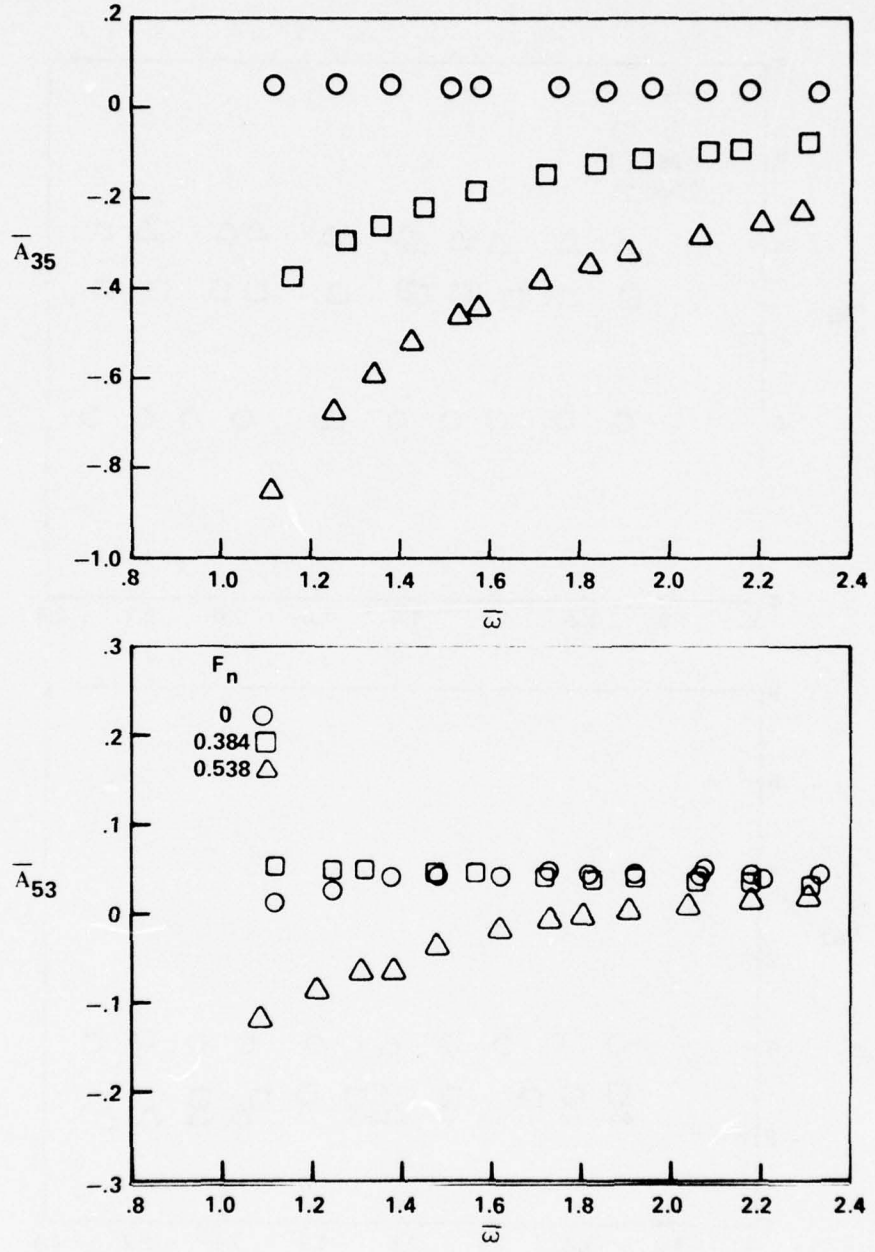

Figure 11c - With Forward Fin and Aft Fin A

Figure 12 - Heave-Pitch Coupling Damping Coefficients versus Frequency for SWATH 6A

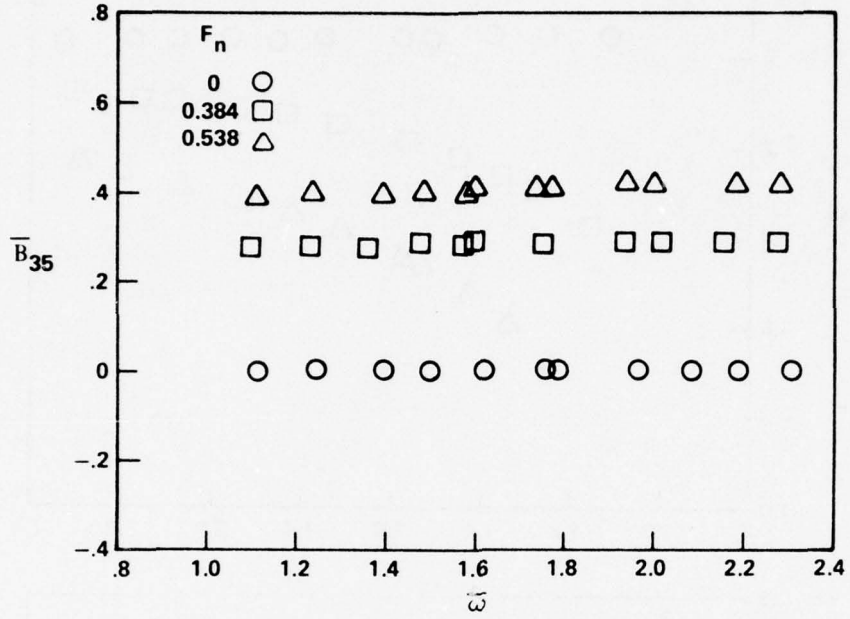

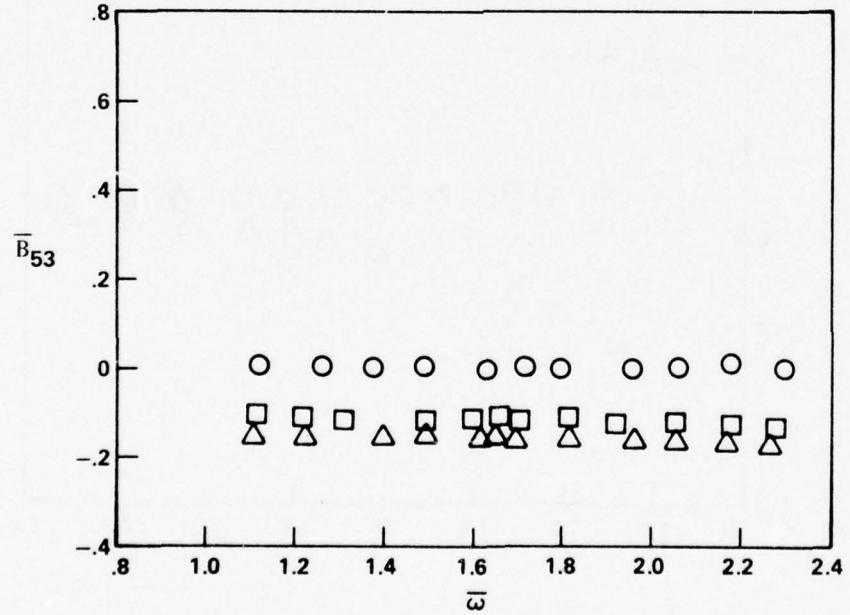

Figure 12a - For Bare Hull

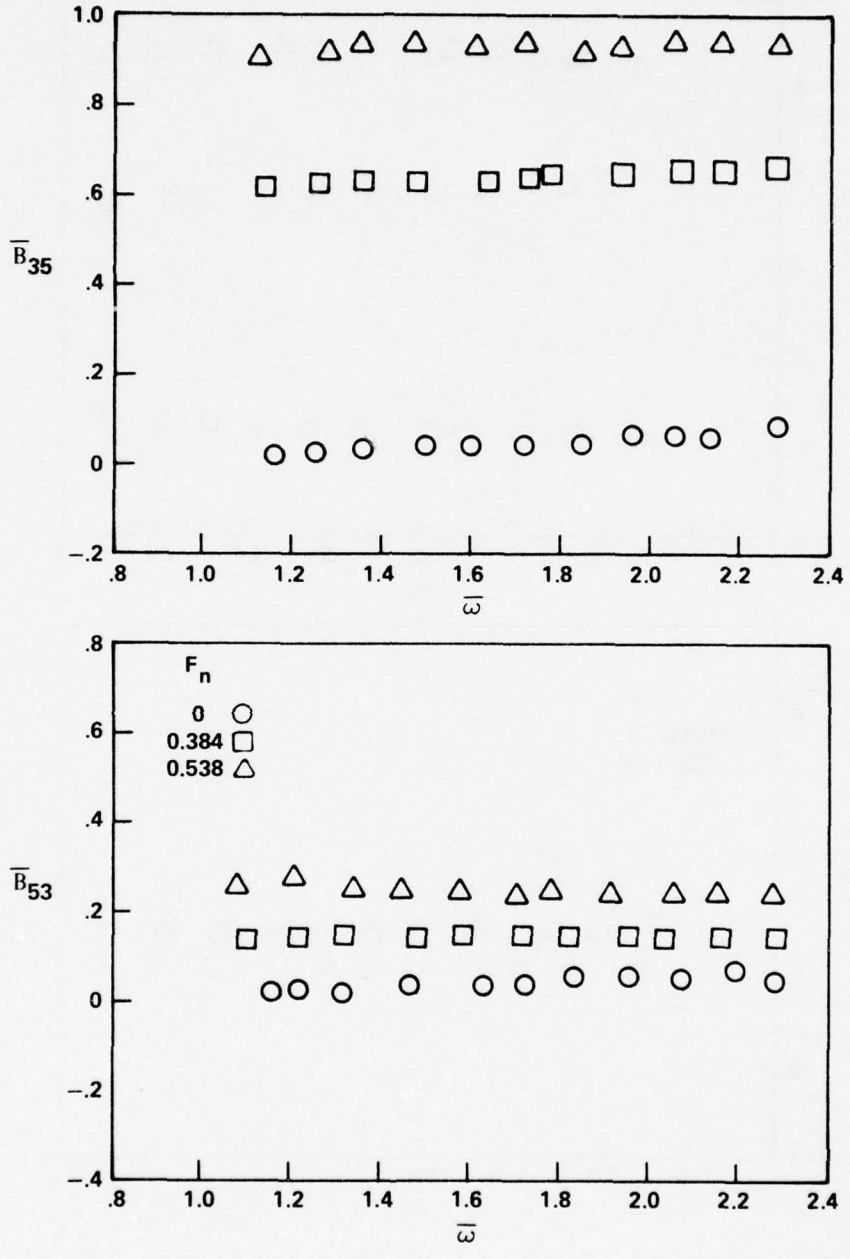

Figure 12b - With Aft Fin A

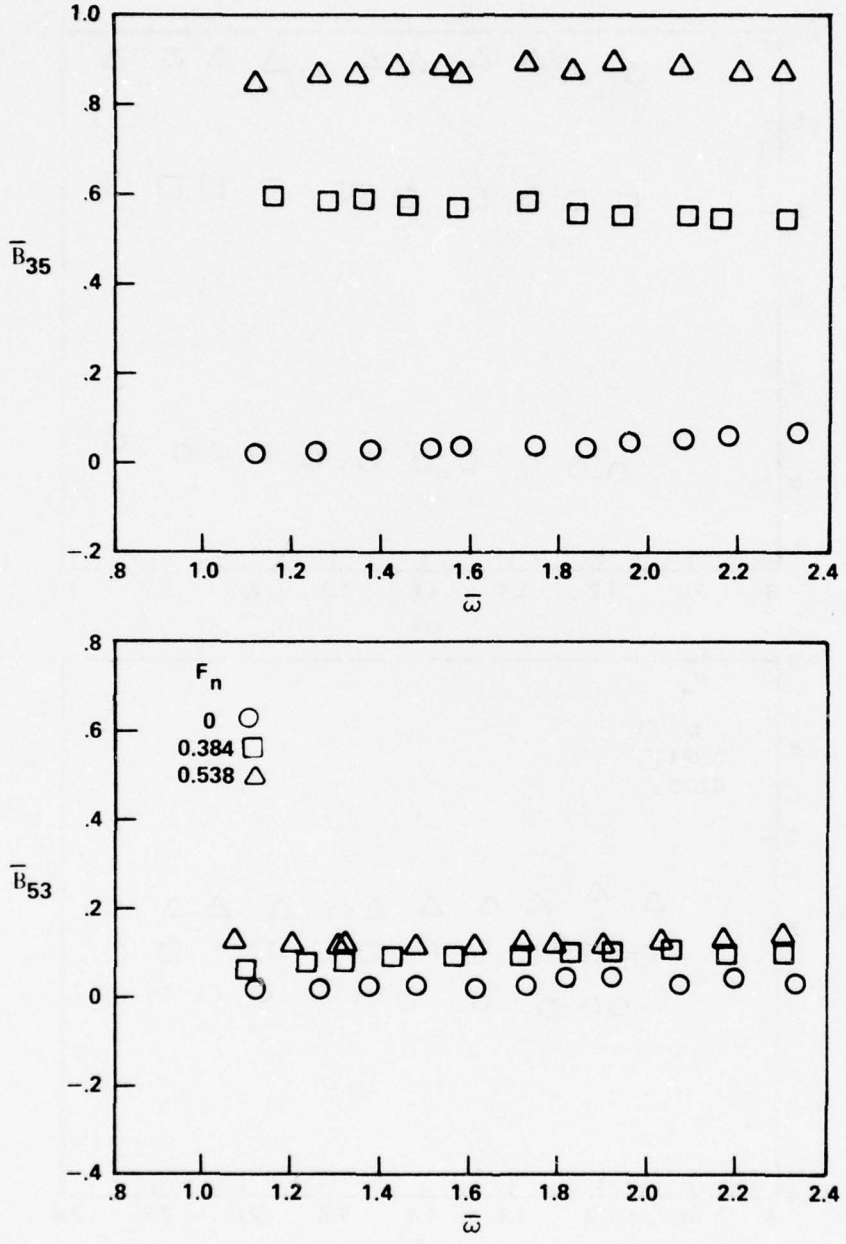

Figure 12c - With Forward Fin and Aft Fin A

Figure 13 - Comparison of Theoretical and Experimental Values of A_{33} and A_{55} for SWATH 6A

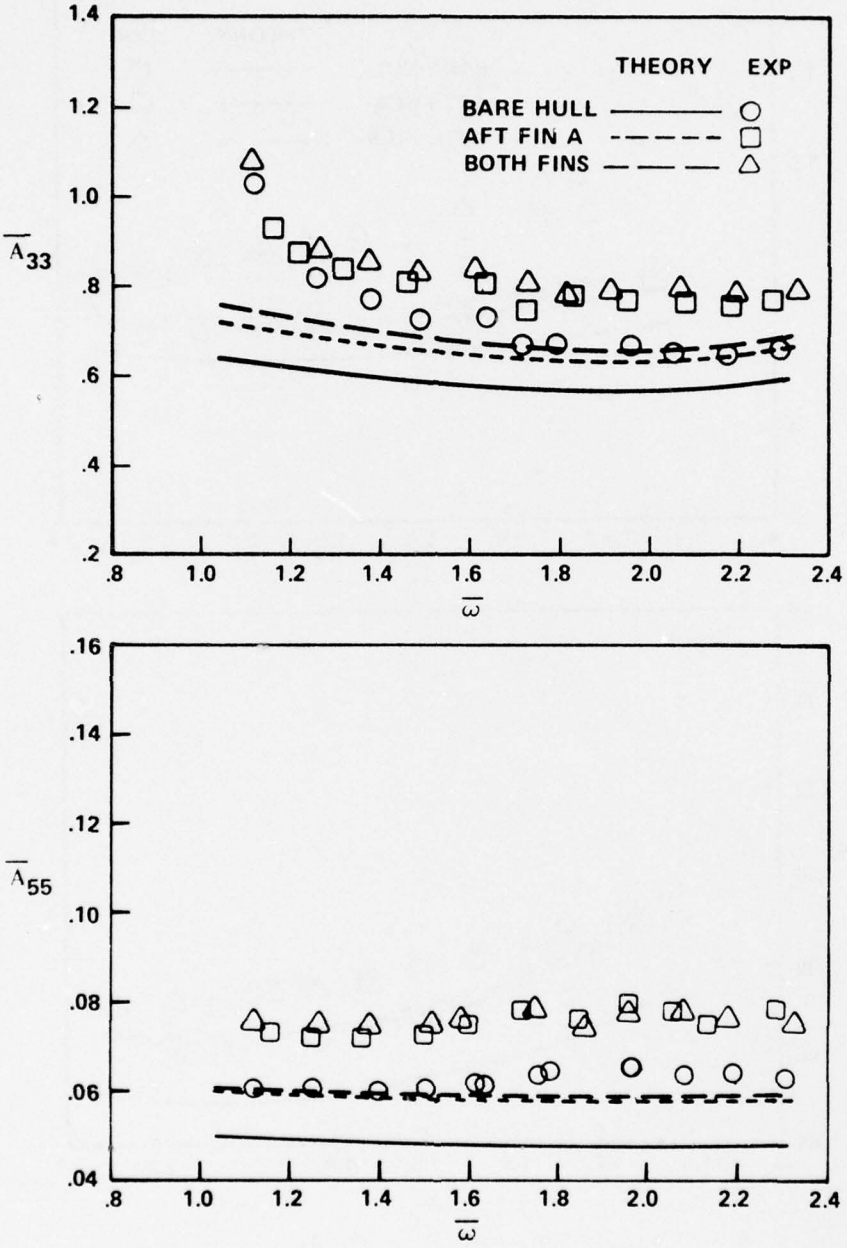

Figure 13a - At $F_n = 0$

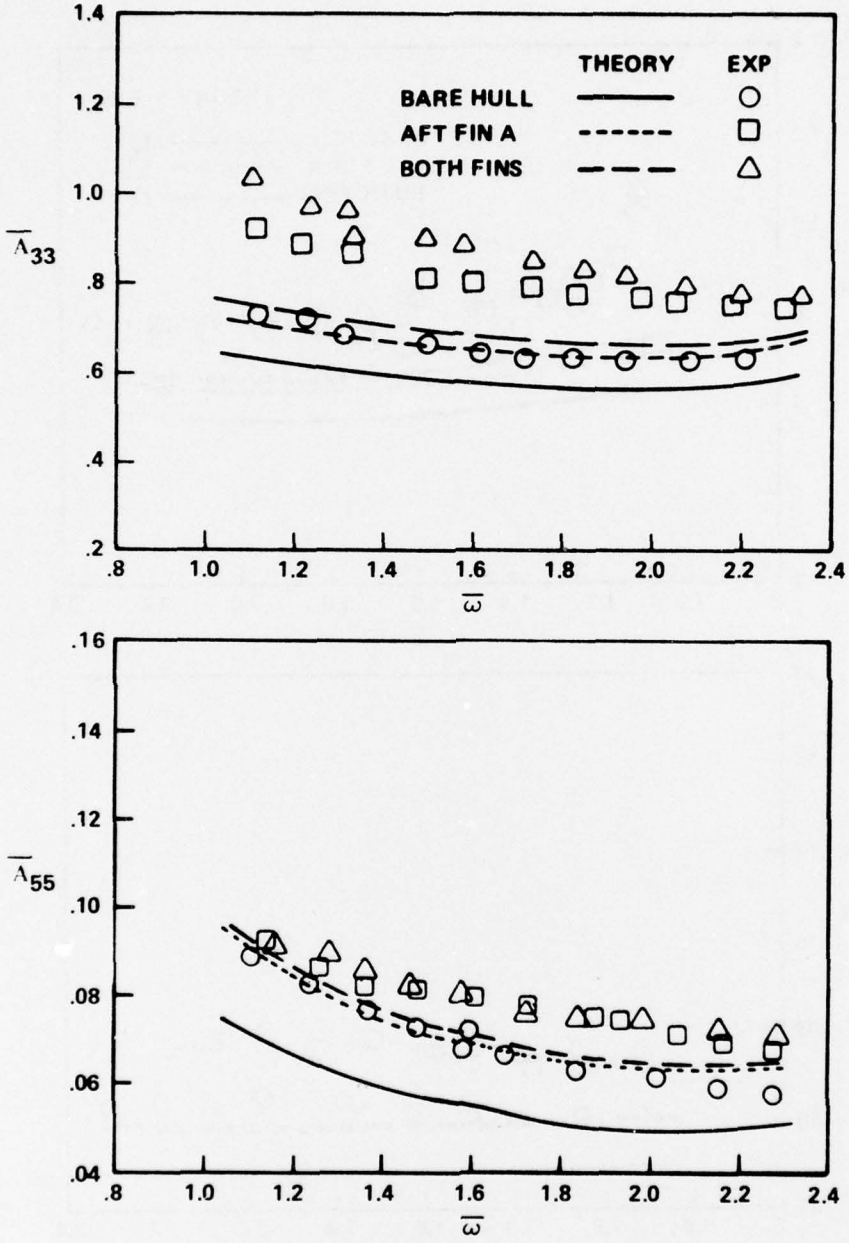

Figure 13b - At $F_n = 0.384$

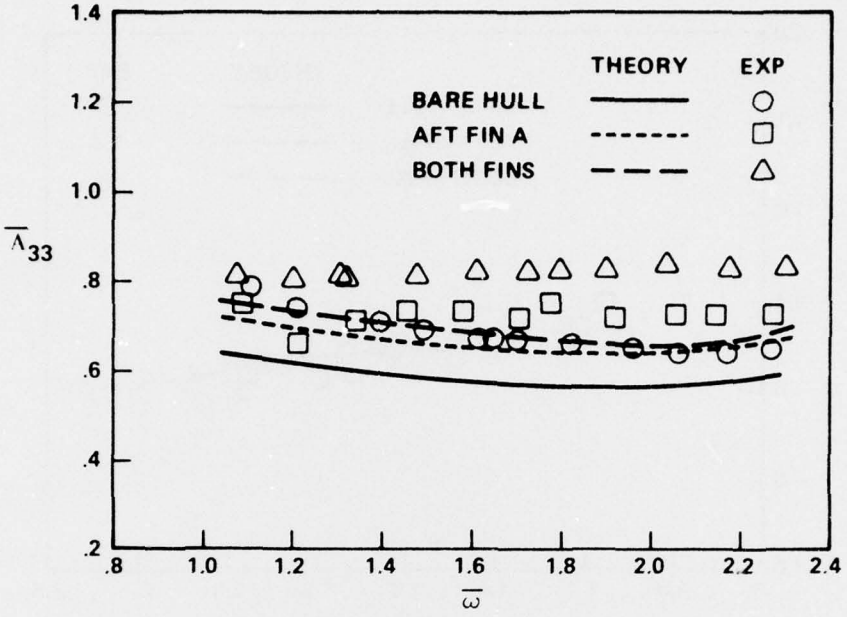

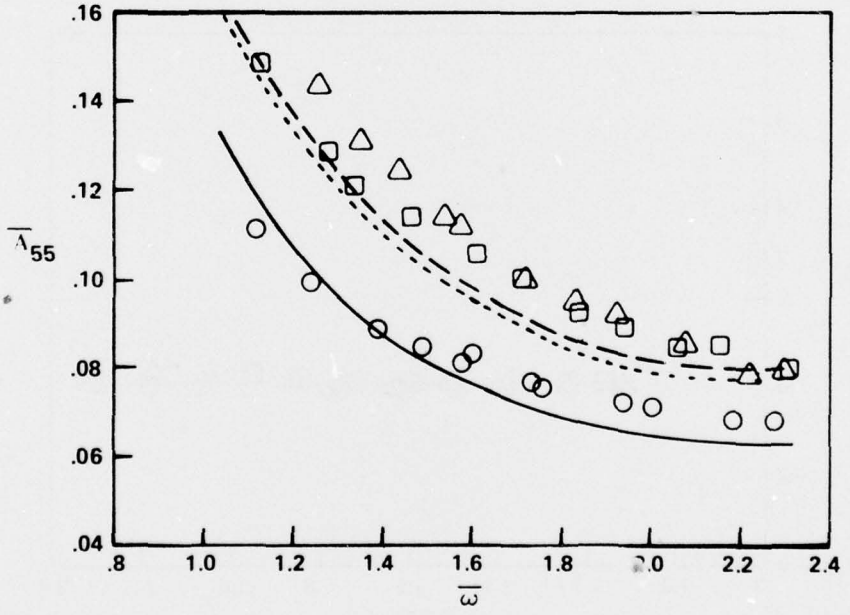

Figure 13c - At F_n = 0.538

Figure 14 - Comparison of Theoretical and Experimental Values of B_{33} and B_{55} for SWATH 6A

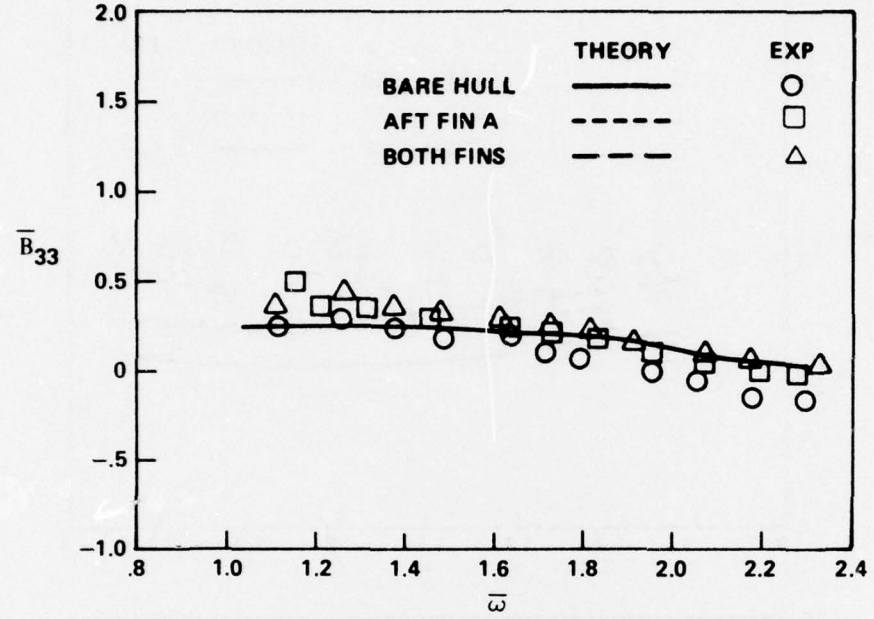

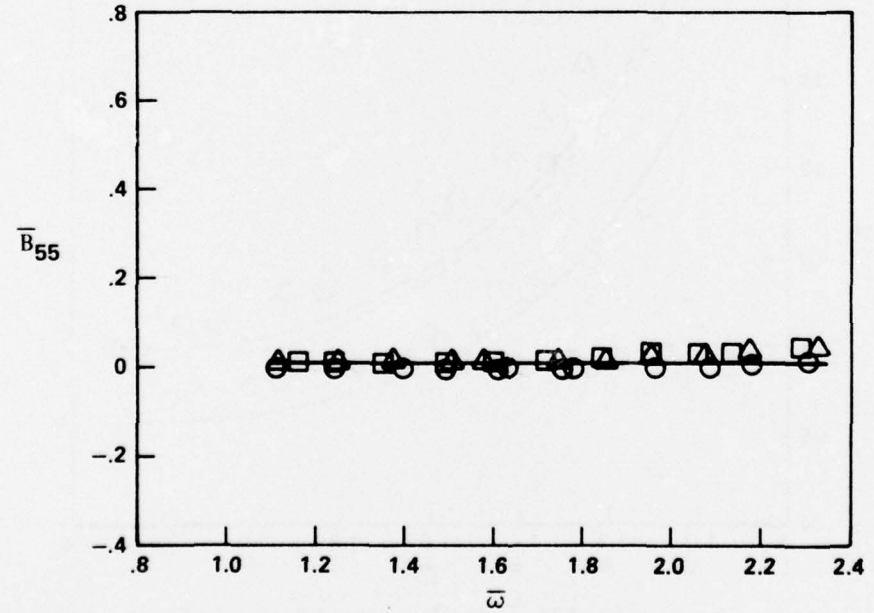

Figure 14a - At $F_n = 0$

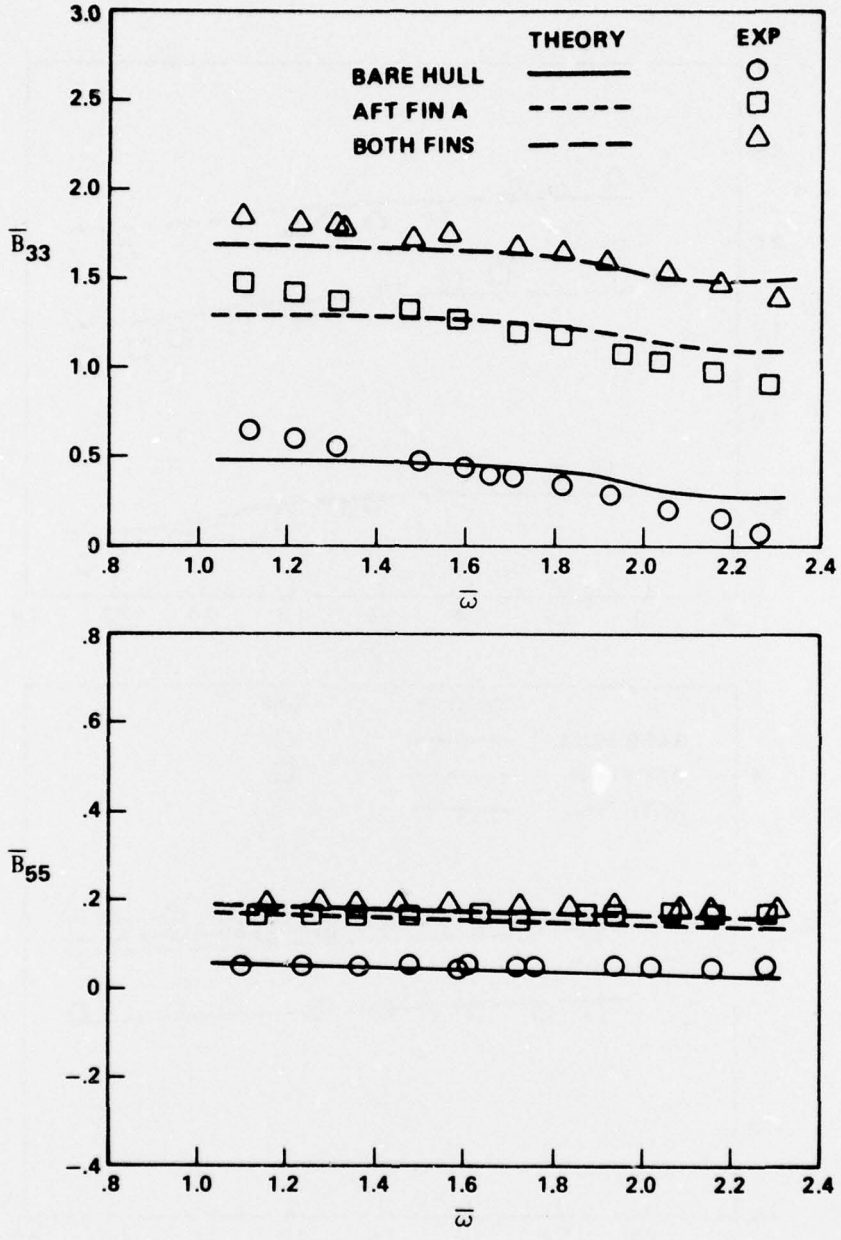

Figure 14b - At $F_n = 0.384$

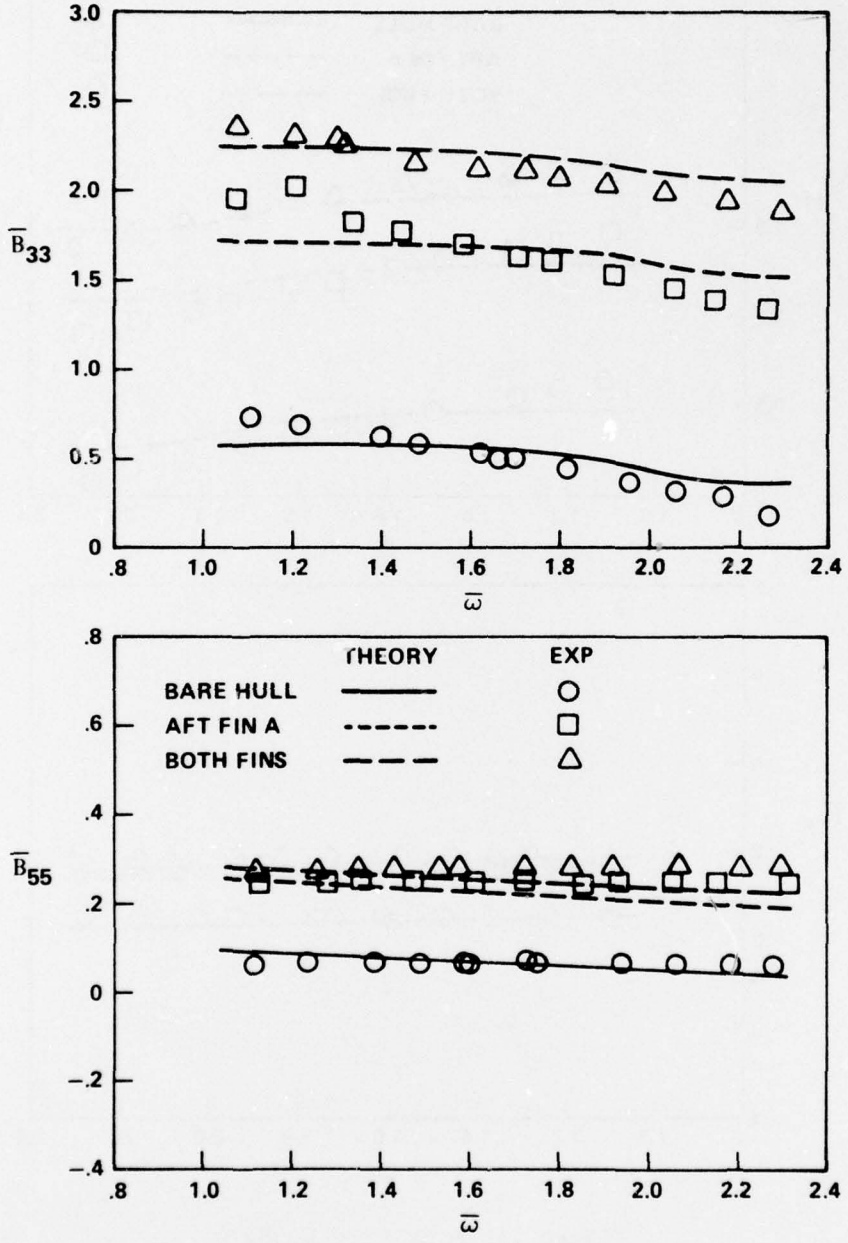

Figure 14c - At F_n = 0.538

Figure 15 - Comparison of Theoretical and Experimental Values of A_{35} and A_{53} for SWATH 6A

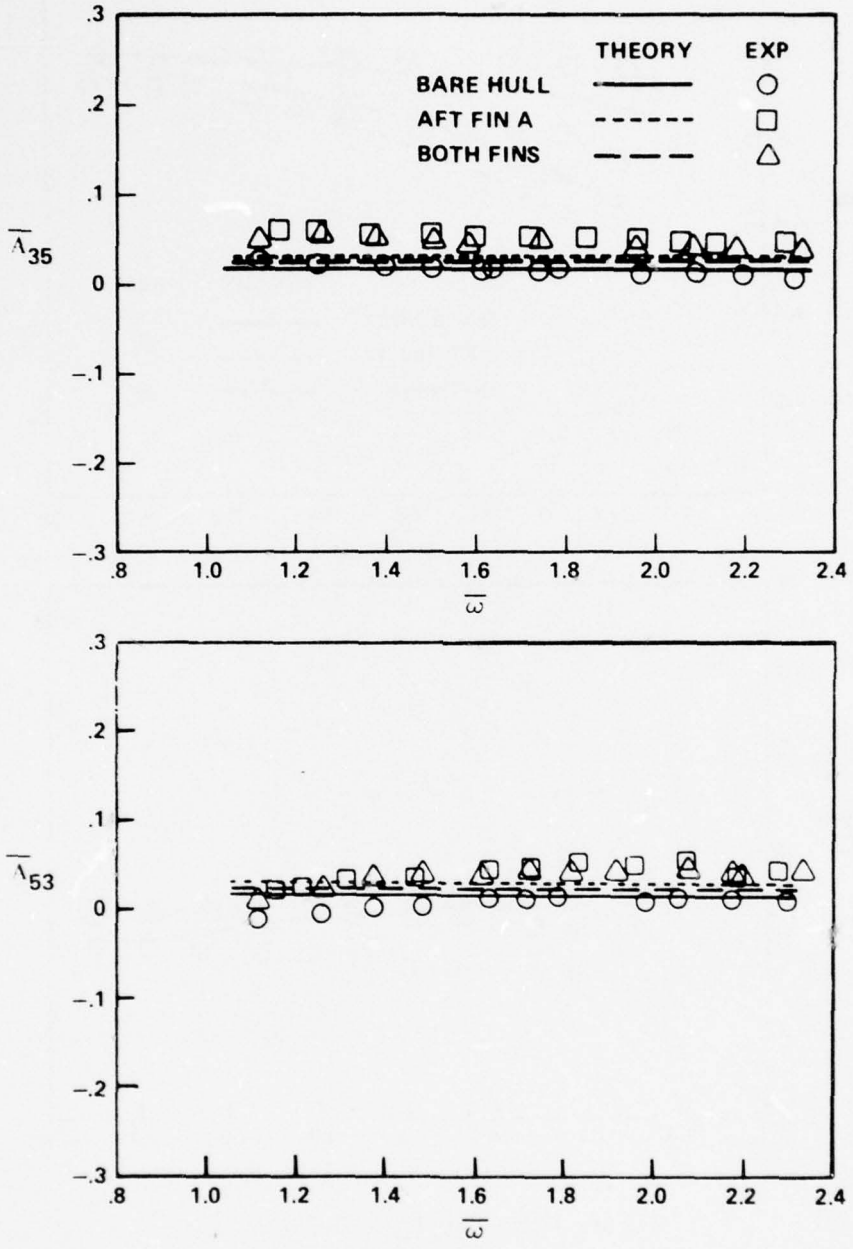

Figure 15a - At $F_n = 0$

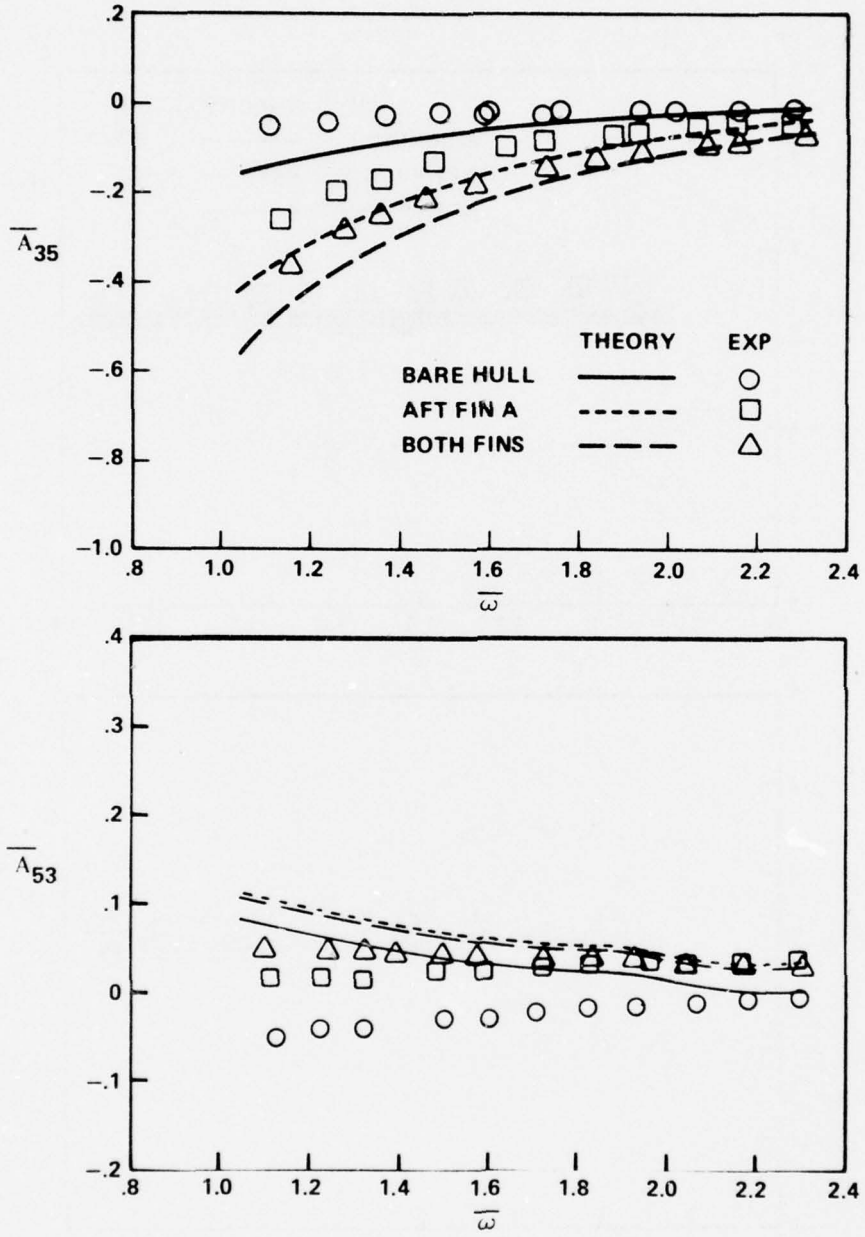

Figure 15b - At F_n = 0.384

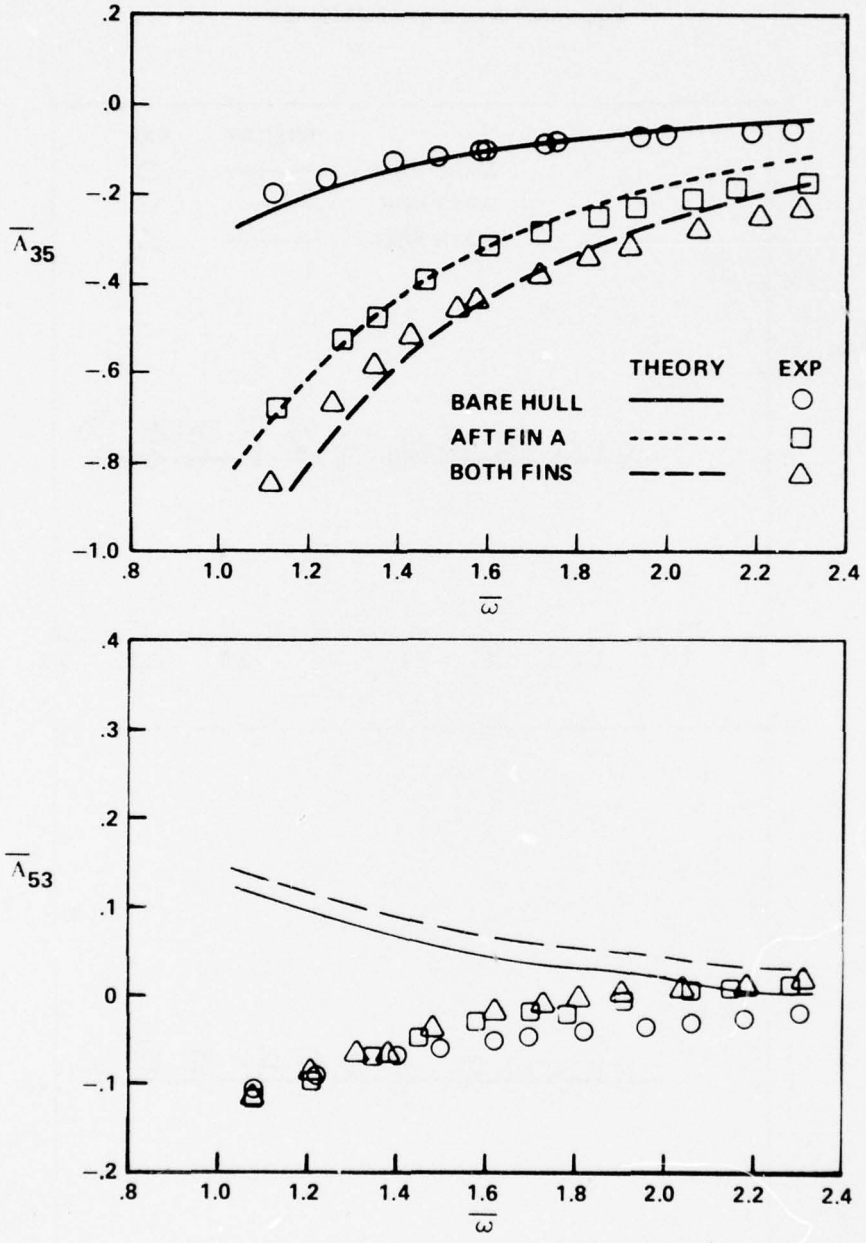

Figure 15c - At F_n = 0.538

Figure 16 - Comparison of Theoretical and Experimental Values of B_{35} and B_{53} for SWATH 6A

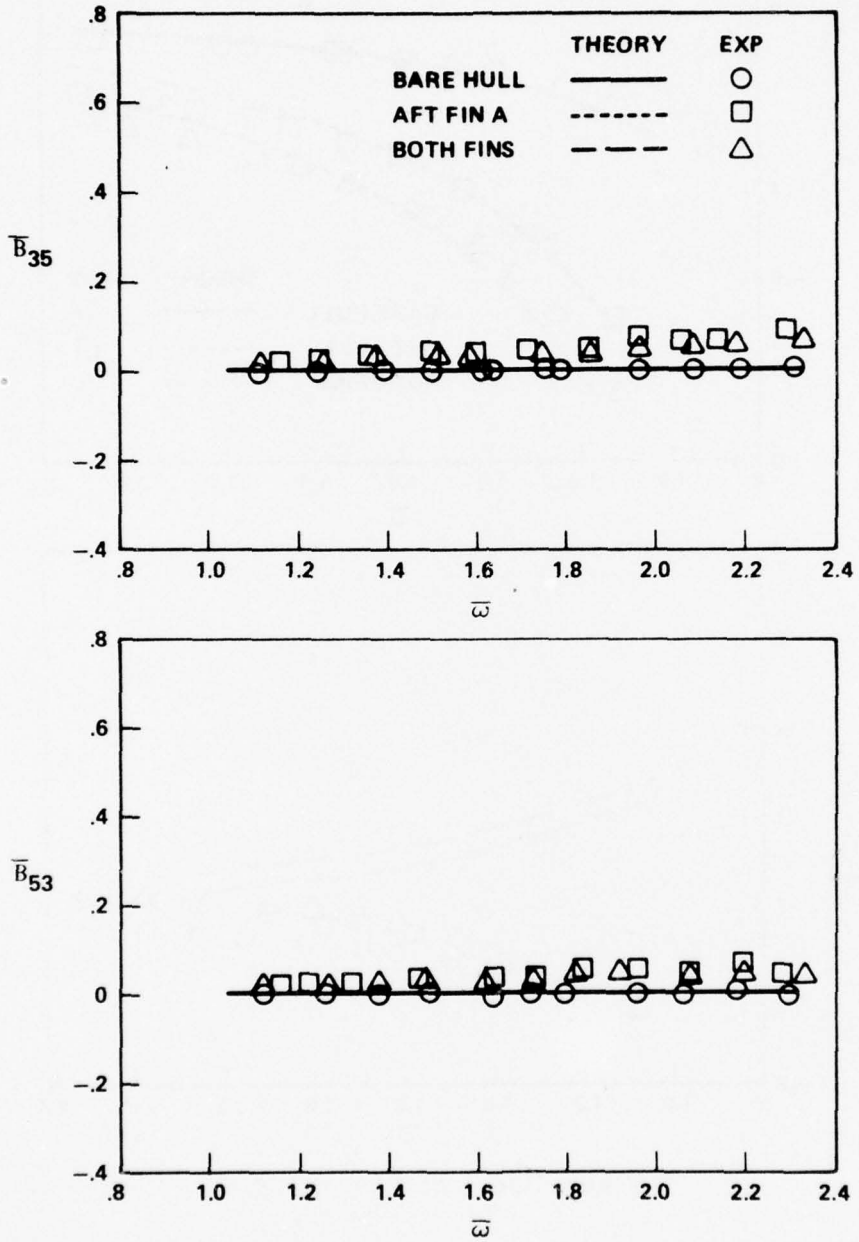

Figure 16a - At $F_n = 0$

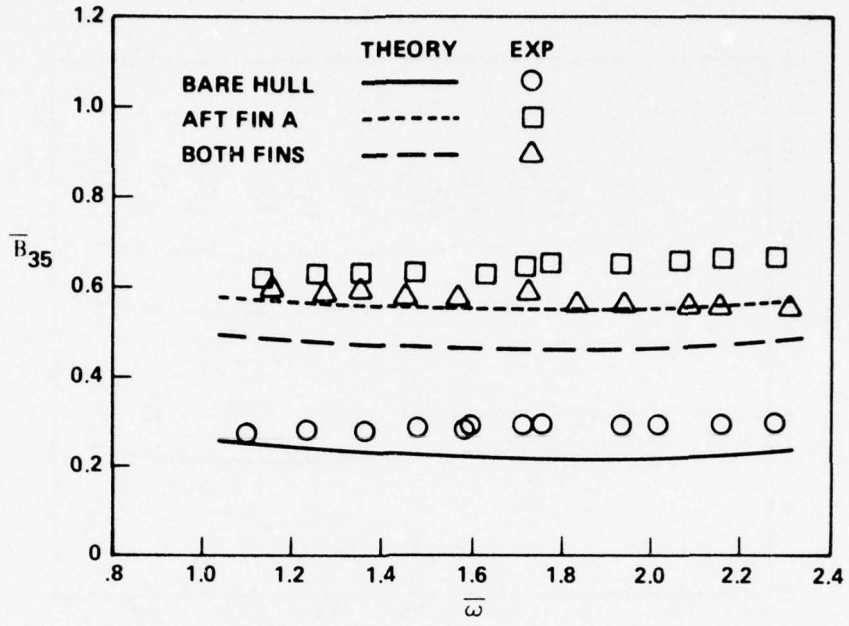

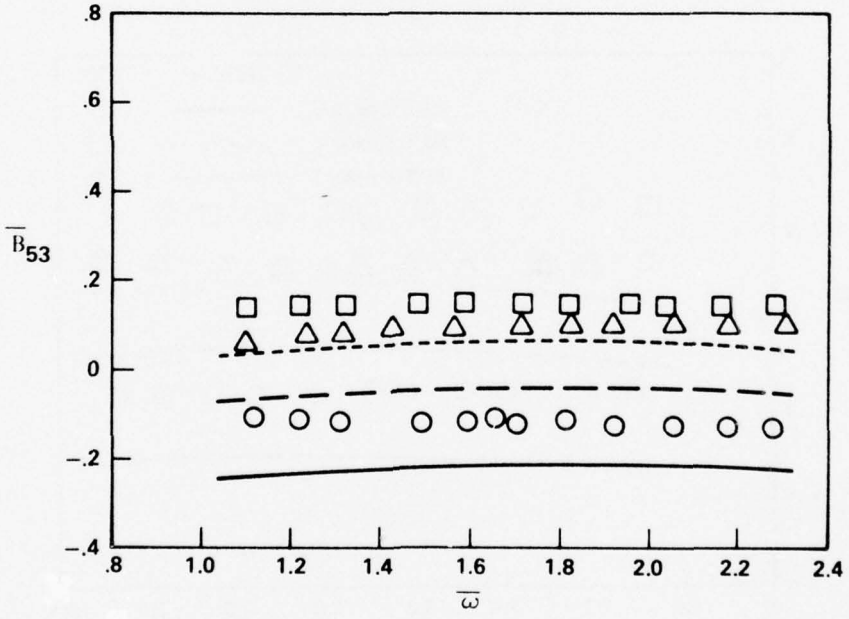

Figure 16b - At $F_n = 0.384$

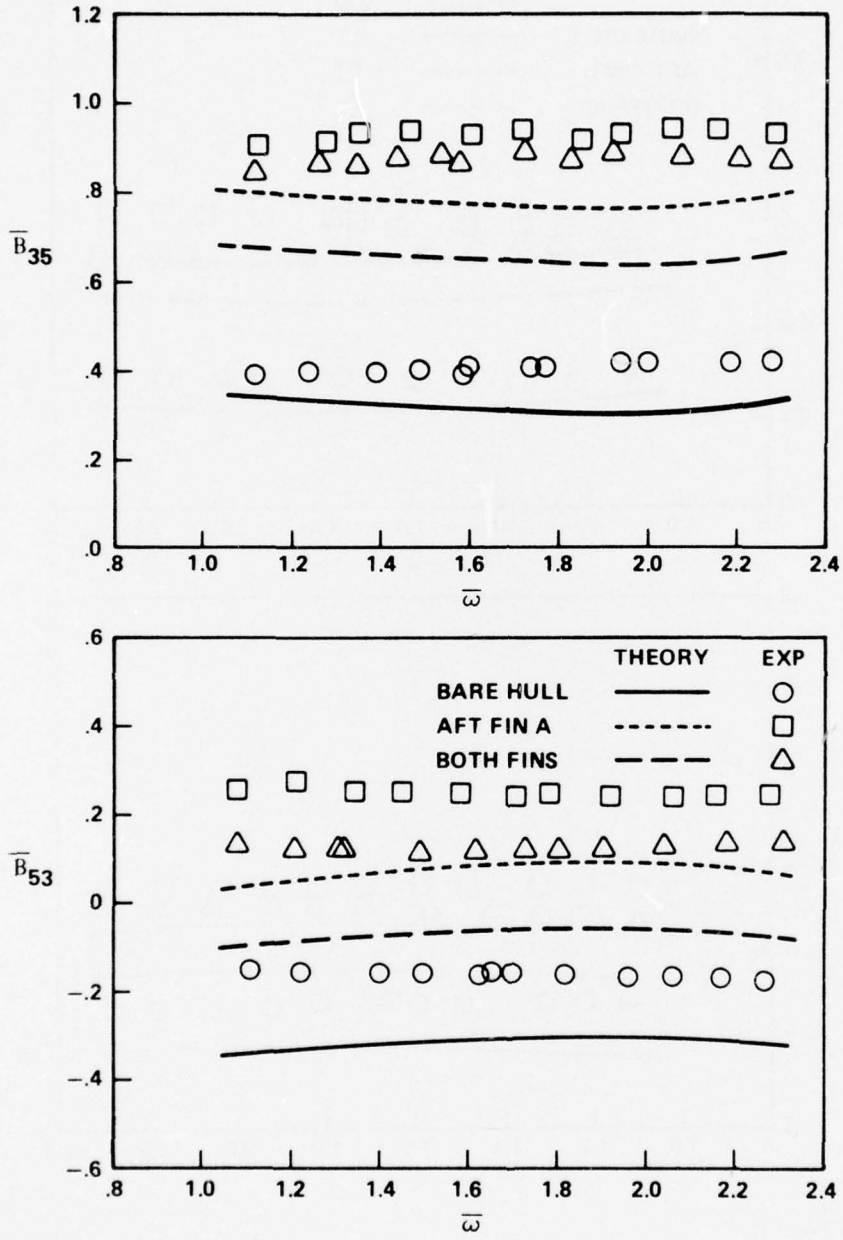

Figure 16c - At F_n = 0.538

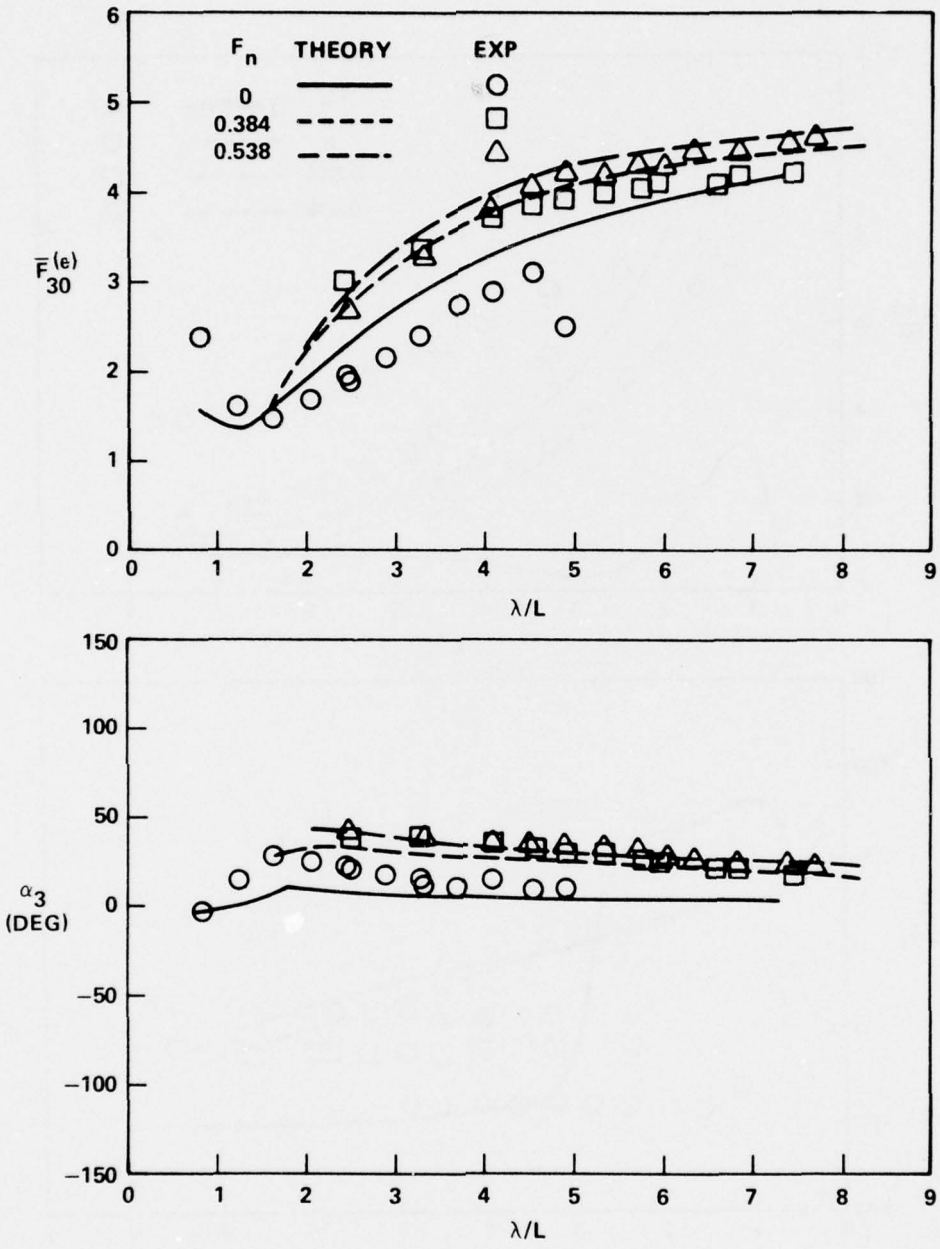

Figure 17 - Comparison of Theoretical and Experimental Amplitudes and Phases of Wave-Exciting Heave Force

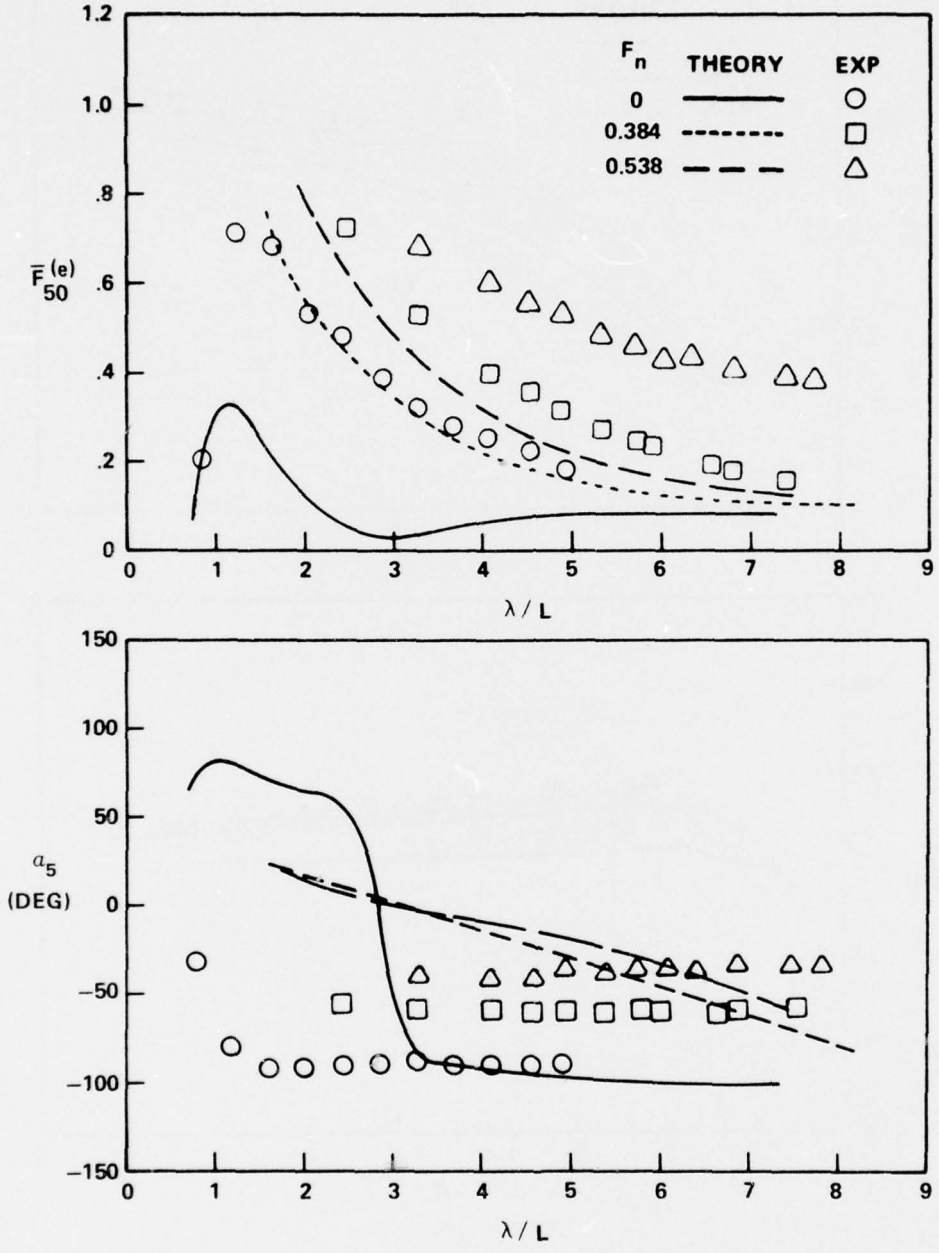

Figure 18 - Comparison of Theoretical and Experimental Amplitudes and Phases of Wave-Exciting Pitch Moment

DTNSRDC ISSUES THREE TYPES OF REPORTS

(1) DTNSRDC REPORTS, A FORMAL SERIES PUBLISHING INFORMATION OF PERMANENT TECHNICAL VALUE, DESIGNATED BY A SERIAL REPORT NUMBER.

(2) DEPARTMENTAL REPORTS, A SEMIFORMAL SERIES, RECORDING INFORMATION OF A PRELIMINARY OR TEMPORARY NATURE, OR OF LIMITED INTEREST OR SIGNIFICANCE, CARRYING A DEPARTMENTAL ALPHANUMERIC IDENTIFICATION.

(3) TECHNICAL MEMORANDA, AN INFORMAL SERIES, USUALLY INTERNAL WORKING PAPERS OR DIRECT REPORTS TO SPONSORS, NUMBERED AS TM SERIES REPORTS; NOT FOR GENERAL DISTRIBUTION.